Eruptive history and geochronology of Mount Mazama and the Crater Lake region, Oregon

Charles R. Bacon†
Marvin A. Lanphere
Volcano Hazards Team, U.S. Geological Survey, MS 910, 345 Middlefield Road, Menlo Park, California 94025, USA

ABSTRACT

Geologic mapping, K-Ar, and $^{40}Ar/^{39}Ar$ age determinations, supplemented by paleomagnetic measurements and geochemical data, are used to quantify the Quaternary volcanic history of the Crater Lake region in order to define processes and conditions that led to voluminous explosive eruptions. The Cascade arc volcano known as Mount Mazama collapsed during its climactic eruption of ~50 km³ of mainly rhyodacitic magma ~7700 yr ago to form Crater Lake caldera. The Mazama edifice was constructed on a Pleistocene silicic lava field, amidst monogenetic and shield volcanoes ranging from basalt to andesite similar to parental magmas for Mount Mazama. Between 420 ka and 35 ka, Mazama produced medium-K andesite and dacite in 2:1 proportion. The edifice was built in many episodes; some of the more voluminous occurred approximately coeval with volcanic pulses in the surrounding region, and some were possibly related to deglaciation following marine oxygen isotope stages (MIS) 12, 10, 8, 6, 5.2, and 2. Magmas as evolved as dacite erupted many times, commonly associated with or following voluminous andesite effusion. Establishment of the climactic magma chamber was under way when the first preclimactic rhyodacites vented ca. 27 ka. The silicic melt volume then grew incrementally at an average rate of 2.5 km³ k.y.⁻¹ for nearly 20 k.y. The climactic eruption exhausted the rhyodacitic magma and brought up crystal-rich andesitic magma, mafic cumulate mush, and wall-rock granodiorite. Postcaldera volcanism produced 4 km³ of andesite during the first 200–500 yr after collapse, followed at ca. 4800 yr B.P. by 0.07 km³ of rhyodacite. The average eruption rate for all Mazama products was ~0.4 km³ k.y.⁻¹, but major edifice construction episodes had rates of ~0.8 km³ k.y.⁻¹. The long-term eruption rate for regional monogenetic and shield volcanoes was ~0.07 km³ k.y.⁻¹, but only ~0.02 km³ k.y.⁻¹ when the two major shields are excluded. Plutonic xenoliths and evidence for crystallization differentiation imply that the amount of magma intruded beneath Mount Mazama is several times that which has been erupted. The eruptive and intrusive history reflects competition between (1) crystallization driven by degassing and hydrothermal cooling and (2) thermal input from a regional magma flux focused at Mazama. Before ca. 30 ka, relatively small volumes of nonerupted derivative magma crystallized to form a composite pluton because the upper crust had not been heated sufficiently to sustain voluminous convecting crystal-poor melt. Subsequently, and perhaps not coincidentally, during MIS 2, a large volume of eruptible silicic magma accumulated in the climactic chamber, probably because of heating associated with mantle input to the roots of the system as suggested by eruption of unusually primitive magnesian basaltic andesite and tholeiite west of Mazama.

Keywords: geochronology, volcanology, argon, calderas, arc volcanism, Crater Lake, Mount Mazama.

INTRODUCTION

Mount Mazama is one of the major volcanoes of the Cascade arc. Although late Pleistocene Mount Mazama was comparable in height (~3700 m) and form to other long-lived Cascade volcanoes, its upper portion collapsed during a rapid climactic series of pyroclastic eruptions ~7700 yr ago, leaving an 8 × 10 km caldera now half-filled by Crater Lake. The geology of the area was first described in detail by Diller and Patton in 1902, the year Crater Lake National Park was established, and later by Williams (1942), whose vivid account led to international recognition of Crater Lake as a classic collapse caldera. Because of good preservation and access, Mount Mazama, Crater Lake caldera, and the deposits formed by the climactic eruption provide excellent opportunities for study of volcanic and magmatic processes. The climactic ejecta are renowned as evidence for systematic compositional zonation within a magma chamber.

The geology and eruptive history of Mount Mazama give insight into how large arc volcanoes can grow over many hundreds of thousands of years. The record is fragmentary because of erosion of Mazama's flanks, blanketing by pyroclastic and glacial deposits, and loss of part of the edifice to caldera collapse. Conversely, the caldera walls provide an incomparable view of the interior of an arc volcano. The Mazama edifice was constructed mainly in discrete episodes, each typically fed by distinct magma, which erupted from vents that migrated westward through time. We sought to quantify the volcano construction process by determining stratigraphic relations and erupted volumes through geologic mapping (Bacon, 2007) and by dating key eruptive units with K-Ar and $^{40}Ar/^{39}Ar$ methods. Results also constrain times of ice presence, as evidenced by buried glaciated surfaces and lava-ice interaction features, which we have compared with independent glacial chronologies. The many smaller volcanoes of the High Cascades beyond the limits of Mount Mazama are a source of information on the flux of mantle-derived magma through the region and presumably into the Mazama magmatic system. We have applied the same approach to these regional lavas near Crater Lake and to silicic lavas protruding from beneath the Mazama edifice. With geochemical data for nearly 1000 samples, we can begin to quantify the time–volume–composition evolution of this long-lived magmatic focus initially outlined by Bacon and Lanphere (1990). Results of comparable studies have been published for only a small number of arc volcanic systems (Hildreth and Lanphere, 1994; Singer et al., 1997; Druitt et al., 1999; Dungan et al., 2001;

†E-mail: cbacon@usgs.gov.

GSA Bulletin; November/December 2006; v. 118; no. 11/12; p. 1331–1359; doi: 10.1130/B25906.1; 7 figures; 2 tables; Data Repository item 2006219.

Thouret et al., 2001; Harford et al., 2002; Hildreth et al., 2003a, 2003b, 2004; Gamble et al., 2003; Frey et al., 2004; Lewis-Kenedi et al., 2005; Jicha and Singer, 2006). Mazama is similar to several of these volcanic fields in many aspects of its eruptive behavior and shares a silicic caldera-forming eruption stage with some. The primary goal of this study was to document the spatial distribution, volume, and composition of eruptive products of Mount Mazama through time and thereby identify factors that led to development of a shallow chamber containing a large volume of silicic magma capable of catastrophic explosive eruption.

This paper reports the K-Ar and $^{40}Ar/^{39}Ar$ geochronologic data, describes the geology, attempts to reconstruct volumes of eruptive units, and interprets the time–volume–composition evolution of the Crater Lake region. In doing this, we draw heavily on the geologic map by Bacon (2007) and, thus, frequently refer to map units that are designated by combinations of bold-face letters (e.g., **db** for dacite of Chaski Bay) to facilitate comparison with the map. We use geochemical data to characterize eruptive units and briefly describe the compositional range found near Crater Lake.

GEOLOGIC OVERVIEW

The Cascade arc is a manifestation of the relatively slow, northeastward subduction of the young, hot Juan de Fuca and Gorda plates beneath the North American plate. The volcanic arc is broad from northern California to southern Washington, where plate convergence is oblique to the continental margin, and is narrow in northern Washington and southern British Columbia, where convergence is normal. Mount Mazama is in the broad part of the arc where there are many smaller *regional* volcanoes that are the surface expression of melts that were born in the mantle and, after undergoing varying amounts of differentiation and assimilation, have escaped readily to the surface because of the mildly extensional tectonic environment at the west edge of the Basin and Range Province. Many regional volcanoes have erupted primitive magmas ranging from high-alumina olivine tholeiite (HAOT; Hart et al., 1984) to magnesian basaltic andesite that reflect increasing amounts of subduction-related fluids or melts added to a depleted mantle source (Bacon, 1990; Bacon et al., 1994, 1997a). The basaltic andesites and more differentiated lavas of Mount Mazama carry geochemical signatures spanning much of the range exhibited by regional primitive magmas.

The underpinnings of Mount Mazama are known from exposures in canyons on its south flank, samples of the submerged caldera walls, and drill cores from two geothermal exploration wells (Bacon and Nathenson, 1996). Extensive Pleistocene dacite and rhyodacite lavas underlie the southern and eastern parts of the edifice (Nakada et al., 1994). Basaltic andesite and andesitic lava flows and shallow intrusions that represent pre-Mazama Quaternary regional volcanism mainly occur west of longitude 122°06′W (approximately the center of the caldera) and form a dissected tableland west of Crater Lake National Park. Near the lake floor off Eagle Point, similar rocks that are hydrothermally altered to greenschist-facies assemblages gave a K-Ar age of 1850 ± 470 ka (Bacon et al., 2002); in the 867-m-deep MZII-1 exploration well, 12 km south of Crater Lake (east of Annie Creek, south of the map boundary), they are comparatively fresh. Beneath pre-Mazama rhyodacite in the MZI-11A exploration well, 7 km southeast of the caldera, there is nearly 1 km of andesitic fragmental rocks and basaltic andesitic lava flows underlain by another 0.4 km of intermediate to silicic tuffs with apparent dips as steep as 36° (Bacon and Nathenson, 1996). The tuffs may correlate with Tertiary rocks of the Western Cascades. Beneath Mazama at a depth of ~5 km is a late Pleistocene composite pluton at least as extensive as the subsided floor of Crater Lake caldera (Bacon and Lowenstern, 2005). The nature of the deeper crust is uncertain. Isotopic data for Mazama area lavas are consistent with involvement of pre-Cenozoic Klamath-type basement rocks but also can be reconciled with contributions from younger mafic rocks (Bacon et al., 1994). Leaver et al. (1984) reported the crust to be 44 km thick ~30 km west of Crater Lake, but crustal thickness beneath Mazama is not well known.

Mount Mazama is somewhat arbitrarily defined as the andesite through dacite edifice built upon older than 400 ka rhyodacitic lavas. The edifice is composed of several overlapping composite and shield volcanoes, each of which was active for a few thousand years, to perhaps 40 ka. Although basaltic andesite erupted intermittently, andesite and dacite were volumetrically dominant. The eruptive focus migrated from the east and southeast to the west. Central vent eruptions apparently ended with dacite dome emplacement ca. 35 ka and were followed from 27 ka into the Holocene by venting of rhyodacitic magma from the growing climactic magma chamber. These preclimactic rhyodacites are thus Mazama magmas, but they did not issue from a central vent (excepting any rhyodacite that may have foundered into the caldera). The climactic eruption occurred ca. 7700 yr. B.P. (see "The Climactic Eruption" section), vented ~50 km^3 of dominantly rhyodacitic magma, and was accompanied by collapse of Crater Lake caldera.

A detailed bathymetric survey of Crater Lake (Bacon et al., 2002) provides a unique record of postcaldera eruptions, the interplay between volcanism and filling of the lake, and sediment transport within this closed basin. Postcaldera volcanoes produced ~4 km^3 of andesite in the first few hundred years after the climactic eruption and a far smaller volume of rhyodacite ca. 4800 yr. B.P.

Active, generally north-south normal faults traverse the Crater Lake region (Bacon et al., 1997b, 1999). All mapped tectonic faults, except those of the east Klamath Lake fault zone, have down-to-the-east normal displacement and apparently little strike-slip motion. Vent alignments, particularly of coeval vents, also tend to be north-south, reflecting the regional maximum horizontal compressive stress (east-west–opening fractures) where not influenced by the Mazama focus.

COMPOSITIONAL OVERVIEW

Magmas erupted in the Crater Lake region range in SiO_2 content from 47.6% to 73.2%. Variation in K_2O with SiO_2 is shown for ~975 U.S. Geological Survey analyses in Figure 1. Products of the climactic eruption are virtually uniform crystal-poor rhyodacite, separated by a compositional gap of 8% SiO_2 from crystal-rich andesite and mafic cumulates. Latest Pleistocene and Holocene preclimactic rhyodacites extend the silicic limit slightly, and their enclaves (undercooled blobs of more mafic magma) overlap the andesite and basaltic andesite of the climactic eruption. The products of the climactic magma chamber are thought to represent rhyodacite derived by crystallization differentiation of various andesitic to basaltic replenishment magmas, plus complementary cumulates (Ritchey, 1980; Bacon and Druitt, 1988; Druitt and Bacon, 1989). Granitoid blocks in the climactic ejecta are Pleistocene Mazama magmas and cumulates that froze at a few kilometers depth (Bacon, 1992; Bacon and Lowenstern, 2005). Postcaldera andesites and rhyodacite appear to represent newly arrived magma and differentiated liquid, respectively (Nelson et al., 1994).

The ~40 pre-Mazama rhyodacite domes and lava flows are both more and less differentiated than climactic rhyodacite and were preceded by dacites; both contain andesitic enclaves (Nakada et al., 1994). Regional lavas are mainly calc-alkalic basaltic andesite but include high-alumina olivine tholeiite and, locally, andesite (Bacon, 1990). Regional lavas have wide ranges of incompatible element concentrations and isotope ratios (Bacon et al., 1994) that indicate contributions from at least two kinds of mantle sources: depleted mantle with an ancient(?)

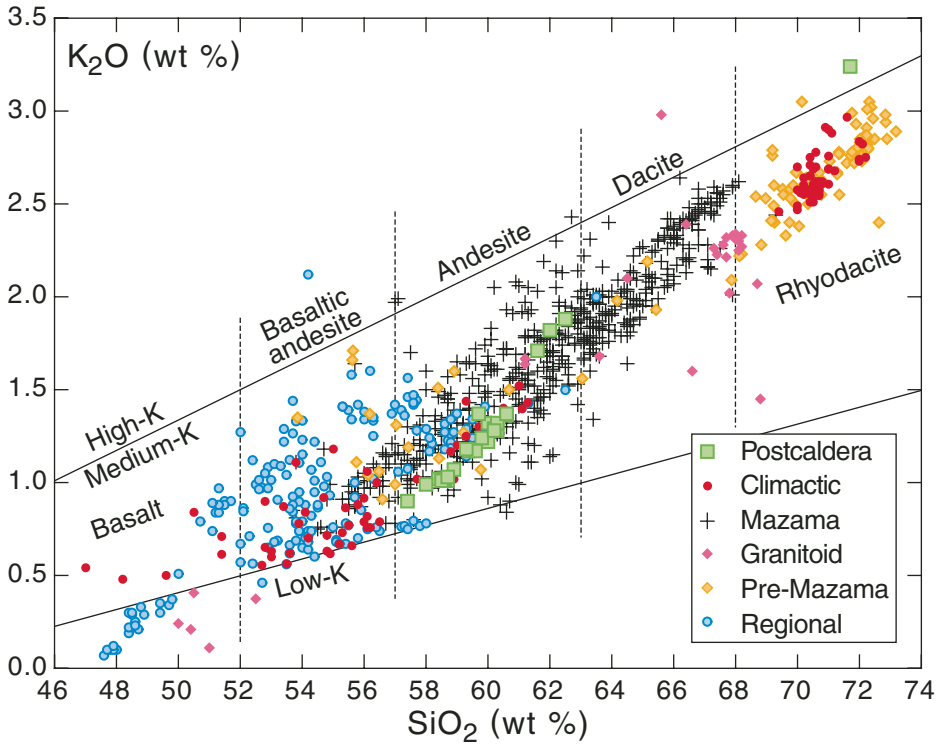

Figure 1. K_2O versus SiO_2 contents (wt%) for ~975 analyses of rocks from the Crater Lake region. Plot groups: postcaldera—andesite lavas and rhyodacite dome; climactic—products of climactic magma chamber including climactic pumice, scoria, and cumulate blocks, as well as preclimactic rhyodacites and enclaves; Mazama—lavas, enclaves, pumice, and juvenile-ejecta blocks composing Mount Mazama; granitoid—0%–50% melted plutonic blocks in climactic ejecta; pre-Mazama—silicic lavas and domes, and their enclaves, underlying Mazama lavas; regional—shield and monogenetic cone lavas. Compositional gap in climactic array extends from 61.3% to 69.4% SiO_2. Major-element analyses were conducted by X-ray fluorescence in Denver, Colorado, U.S. Geological Survey (USGS) laboratory and have been recalculated to sum to 100% volatile-free. Data are from Bruggman et al. (1987, 1989, 1993) and C.R. Bacon (2005, unpublished data). Low-, medium-, and high-K field boundaries have been extended from Gill (1981). Basalt, basaltic andesite, andesite, dacite, and rhyodacite classification is based on SiO_2 content as in previous work at Crater Lake (Bacon, 2007).

subduction component (the high-alumina olivine tholeiite source) and domains enriched in elements mobile in subduction-related fluids of the Cascade arc (Bacon et al., 1997a).

The cloud of Mazama edifice data in Figure 1 spans 54%–68% SiO_2 and largely fills the compositional gap in the climactic ejecta. Most intermediate to silicic Mazama eruptives are porphyritic (commonly 20%–40% phenocrysts) and typically contain small fragments of recycled plutonic rock or cumulate mush (Bacon, 2007). Andesitic or basaltic andesitic enclaves formed by mingling and undercooled crystallization of relatively hot magma in more silicic, cooler host magma are common in many units (Bacon, 1986). More thoroughly mixed hybrid magmas also are common. Parental melts evidently owed their chemistry to variable degrees of melting and subduction-component enrichment in the mantle, and this is reflected in the threefold range in K_2O concentration among andesites. With few exceptions, the incompatible element range diminishes beyond ~64% whole-rock SiO_2. Although several trends and clusters related to specific units are evident within the Mazama edifice data (Fig. 1), space does not permit separating and evaluating them here.

The dominant phenocryst assemblage in Mazama eruptives is plagioclase + augite + orthopyroxene + Fe-Ti oxide. Olivine is present in many samples, and ilmenite is present in rhyodacites and some dacites. Hornblende is conspicuous in basaltic andesite of Hillman Peak, andesite of Garfield Peak, climactic andesite and mafic scoria, and evolved Pleistocene preclimactic rhyodacite, as well as in most other rhyodacites, and in sparse amounts in a few andesitic units. Apatite commonly occurs as needles included in all phenocryst phases (except olivine) in andesites and more silicic rocks (Bacon, 1989). Polycrystalline aggregates derived from plutonic rock, or from crystal mush in which intergranular glass remains, typify pre-Mazama silicic rocks, many Mazama products, and some regional lavas, particularly those that vented close to Mazama. Many phenocrysts in lavas are derived from microxenoliths or aggregates, and some microphenocrysts probably originated in enclaves (Nakada et al., 1994), although some lavas have seriate textures that appear to reflect partial crystallization of melt without extensive admixing of mush or country rock debris.

METHODS

Whole-rock compositions were determined by U.S. Geological Survey (USGS) laboratories. Major oxide contents from X-ray fluorescence analyses were recalculated to sum to 100% volatile-free; in the text, SiO_2 values were rounded to the nearest 0.5%. Rock names are based on silica content: basalt, ≤52%; basaltic andesite, 52–57%; andesite, 57–63%; dacite, 63–68%; and rhyodacite, 68–73%. Phenocryst contents are visual estimates. The Holocene-Pleistocene boundary is 10 ka; late Pleistocene–middle Pleistocene boundary, 128 ± 1 ka (Stirling et al., 1998); and middle Pleistocene–early Pleistocene boundary, 775 ± 10 ka (Bassinot et al., 1994). In the context of lava-ice contact features (e.g., Lescinsky and Fink, 2000) and buried glaciated surfaces, we refer to marine oxygen isotope stages (MIS; Bowen et al., 1986; Martinson et al., 1987; Bassinot et al., 1994) and the Last Glacial Maximum (LGM; ca. 22–16 ka near Crater Lake; Rosenbaum and Reynolds, 2004).

Geologic mapping was recorded in the field on aerial photographs. Unit contacts and generalized caldera wall geology were transferred to a stable topographic base using a Kern PG-2 stereoplotter, scanned, and edited with ArcInfo GIS software using the ALACARTE interface (Fitzgibbon and Wentworth, 1991; Wentworth and Fitzgibbon, 1991). The caldera floor was mapped in ALACARTE/ArcInfo on a base created from the digital elevation model (DEM) obtained in the 2000 multibeam echo-sounding bathymetric survey (Gardner et al., 2001; Bacon et al., 2002). The combined data form the geologic map (Fig. 2). A companion shaded relief map shows morphologic features and place names (Fig. 3). The geology of the caldera walls was mapped on photographs taken from Crater Lake, Wizard Island, and a helicopter, transferred to panoramic views made from photomosaics, and combined with topographic contours determined from a DEM (Fig. 4). A 1:24,000-scale geologic map of surficial deposits and

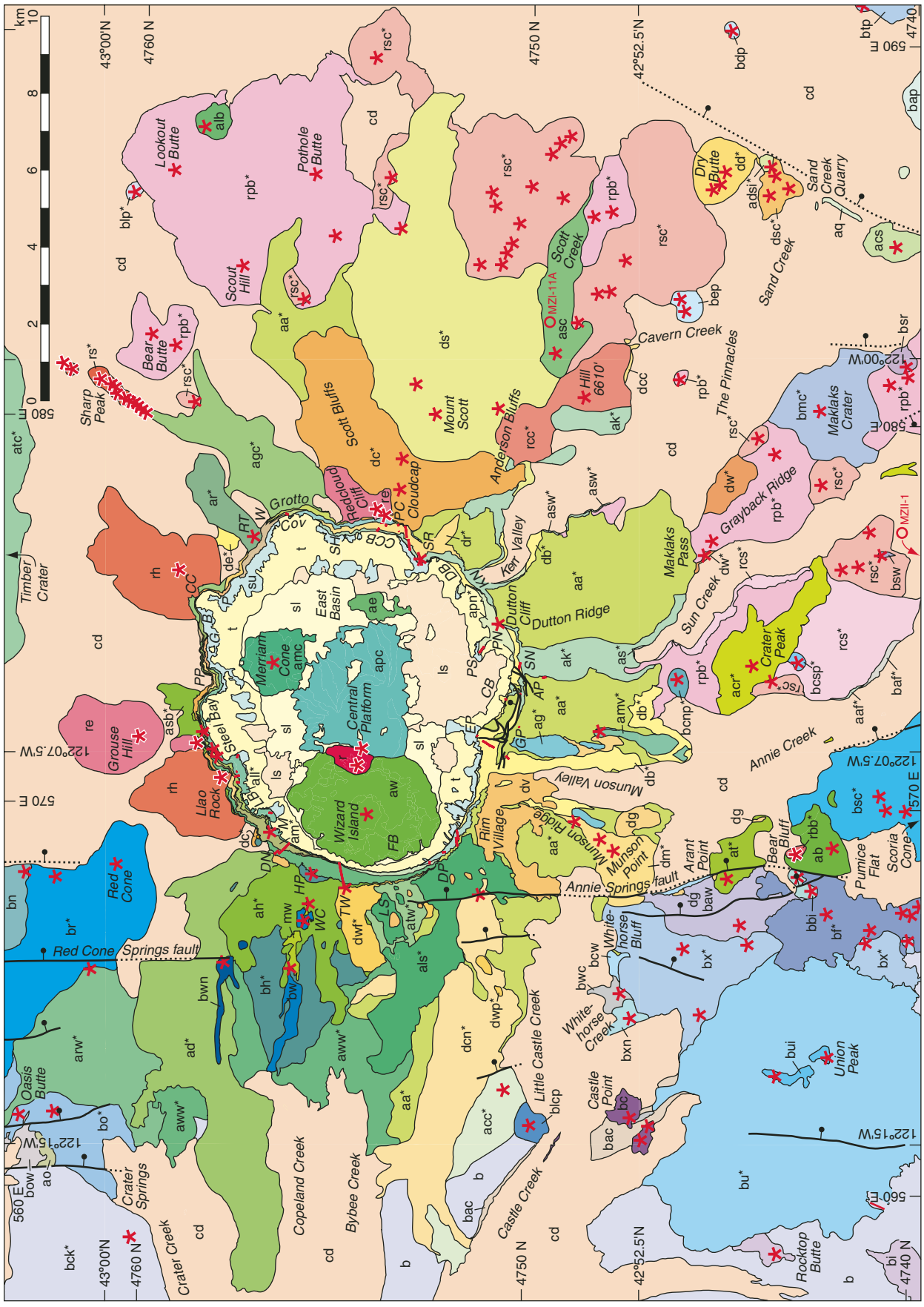

Figure 2 (*on this and following page*). **Geologic map of Mount Mazama and surrounding region, adapted from interpretive bedrock map (Bacon, 2007) in which glacial and thin pyroclastic deposits are not shown. See Figure 3 caption for explanation of place names. Asterisks by unit labels in explanation indicate units dated by K-Ar or $^{40}Ar/^{39}Ar$. First letters of volcanic unit labels indicate composition: b—basalt or basaltic andesite; a—andesite; d—dacite; r—rhyodacite. Tick marks at edge of map are latitude, longitude, and UTM Zone 10 Eastings and Northings (km).**

LIST OF MAP UNITS

[Units shown on maps and (or) panoramas]

SURFICIAL DEPOSITS

- sl — Sediment gravity-flow deposits (Hol.)
- t — Talus (Hol. and Pleist.)
- ls — Landslide deposits (Hol.)
- g — Glacial deposits, undivided (Pleist.)
- s — Sedimentary deposits, undivided (l. and m. Pleist.)

VOLCANIC ROCKS

Mount Mazama

- r — Rhyodacite of the postcaldera dome (Hol.)
- aw — Andesite of Wizard Island (Hol.)
- amc — Andesite of Merriam Cone (Hol.)
- apc — Andesite of the central platform (Hol.)
- ae — Andesite of the E basin (Hol.)
- cd — Deposits of the climactic eruption (Hol.)
- Hol. preclimactic rhyodacite (Hol.)
  - rh — Lava
  - rhp — Pyroclastic
- rs* — Rhyodacite of Sharp Peak (l. Pleist.)
- ab — Andesite S of Bear Bluff (l. Pleist.)
- rbb* — Rhyodacite of Bear Bluff (l. Pleist.)
- re — Evolved Pleist. preclimactic rhyodacite (l. Pleist.)
- mw — Mingled lava of Williams Crater (l. Pleist.)
- dv — Dacite of Munson Valley (l. Pleist.)
- als* — Andesite of Lightning Spring (l. Pleist.)
- asb* — Andesite of Steel Bay (l. Pleist.)
- apu* — Andesite of Pumice Point (l. Pleist.)
- ad* — Andesite of Devils Backbone (l. Pleist.)
- atw — Andesite S of The Watchman (l. Pleist.)
- Dacite of The Watchman (l. Pleist.)
  - dwf* — Lava
  - dwp — Pyroclastic-flow deposits
- ah* — Andesite of Hillman Peak (l. Pleist.)
- dlp — Dacite below Llao Rock (l. Pleist.)
- agc* — Andesite of Grotto Cove (l. Pleist.)
- bh* — Basaltic andesite of Hillman Peak (l. Pleist.)
- Dacite of Pumice Castle (l. Pleist.)
  - dc* — Lava
  - dcp — Pyroclastic
- bs — Basaltic andesite of Steel Bay (l. Pleist.)
- apw — Andesite W of Pumice Point (l. Pleist.)
- aww* — Andesite of the W wall (l. Pleist.)
- arw* — Andesite W of Red Cone (l. Pleist.)
- su* — Submerged caldera wall outcrops, undiv. (Pleist.)
- abl* — Andesite of the Boat Landing (l. Pleist.)
- dpe* — Dacite E of Palisade Point (l. Pleist.)
- Dacite of Steel Bay (l. Pleist.)
  - dsb* — Lava
  - dsbp — Pyroclastic
- am* — Andesite of Merriam Point (l. Pleist.)
- alu* — Andesite of Llao Bay, upper unit (l. Pleist.)
- dpt — Dacite of Palisade Point (l. or m. Pleist.)
- all* — Andesite of Llao Bay, lower unit (m. Pleist.)
- ar* — Andesite of Roundtop (m. Pleist.)
- amv* — Andesite E of Munson Valley (m. Pleist.)
- ags* — Andesite of the gauging station (m. Pleist.)
- dcn* — Dacite N of Castle Creek (m. Pleist.)
- ag* — Andesite of Garfield Peak (m. Pleist.)
- dg — Dacite S of Garfield Peak (m. Pleist.)
- aa* — Andesite of Applegate Peak (m. Pleist.)
- awe — Andesite E of Wineglass (m. Pleist.)
- ac* — Andesite of Cloudcap Bay (m. Pleist.)
- dm* — Dacite of Munson Ridge (m. Pleist.)
- af* — Andesite W of Fumarole Bay (m. Pleist.)
- arv* — Andesite below Rim Village (m. Pleist.)
- dr* — Dacite of Sentinel Rock (m. Pleist.)
- ak* — Andesite of Kerr Notch (m. Pleist.)
- db* — Dacite of Chaski Bay (m. Pleist.)
- dpn — Dacite of Phantom Cone (m. Pleist.)
- ds* — Dacite of Mount Scott (m. Pleist.)
- dcc — Dacite of Cavern Creek (m.? Pleist.)
- apn* — Andesite of Phantom Cone (m. Pleist.)

Regional Volcanism, East

- asc* — Andesite of Scott Creek (l. Pleist.)
- acr* — Andesite of Crater Peak (l. Pleist.)
- bcsp* — Basaltic andesite S of Crater Peak (l. Pleist.)
- bcnp* — Basaltic andesite N of Crater Peak (m.? Pleist.)
- alb* — Andesite S of Lookout Butte (m. Pleist.)
- bsw — Basalt W of Sun Creek (m. Pleist.)
- bmc* — Basaltic andesite of Maklaks Crater (m. Pleist.)
- bsr — Basalt of Sand Ridge (m. Pleist.)
- btp — Basaltic andesite NE of Boundary Butte (m. Pleist.?)
- rpb* — Rhyodacite of Pothole Butte (m. Pleist.)
- rcs — Rhyodacite S of Crater Peak (m. Pleist.)
- rsc* — Rhyodacite of Scott Creek (m. Pleist.)
- aq — Andesite of Sand Creek quarry (m.? Pleist.)
- aaf* — Andesite NE of Annie Falls (m. Pleist.)
- bep — Basaltic andesite E of Cavern Creek (m.? Pleist.)
- acs — Andesite S of Sand Creek (m.? Pleist.)
- bdp — Basaltic andesite E of Dry Butte (m.? Pleist.)
- bap — Basaltic andesite of Boundary Butte (m.? Pleist.)
- as* — Andesite of Sun Creek (m. Pleist.)
- dw* — Dacite W of The Pinnacles (m. Pleist.)
- blp* — Basaltic andesite N of Lookout Butte (m. Pleist.)
- asw* — Andesite W of Sand Creek (m. Pleist.)
- baf* — Basaltic andesite E of Annie Falls (m. Pleist.)
- rcc* — Rhyodacite W of Cavern Creek (m. Pleist.)
- dsc* — Dacite of Sand Creek (e. Pleist.)
- adsi* — Andesite S of Dry Butte (e. Pleist.)
- dd* — Dacite of Dry Butte (e. Pleist.)

Regional Volcanism, Northwest

- bwn — Basaltic andesite NW of Williams Crater (l. Pleist.)
- bw — Basaltic andesite of Williams Crater (l. Pleist.)
- br* — Basaltic andesite of Red Cone (l. Pleist.)
- atc* — Andesite of Timber Crater (l. or m. Pleist.)
- bo — Basaltic andesite of Oasis Butte (m. Pleist.)
- bn — Basaltic andesite N of Red Cone (m.? Pleist.)
- ao — Andesite SW of Oasis Butte (m. Pleist.)
- bow — Basaltic andesite W of Oasis Butte (m.? Pleist.)
- bck* — Basaltic andesite N of Crater Creek (e. Pleist.)

Regional Volcanism, Southwest

- bc — Basalt of Castle Point (e. Hol.)
- blcp — Basaltic andesite N of Little Castle Creek (l. Pleist.)
- bsc* — Basaltic andesite of Scoria Cone (l. Pleist.)
- bf* — Basaltic andesite NW of Pumice Flat (l. Pleist.)
- Basaltic andesite of Union Peak (m. Pleist.)
  - bu* — Lava
  - bui — Intrusive
- bx* — Basaltic andesite of Whitehorse Bluff (m. Pleist.)
- at* — Andesite of Arant Point (m. Pleist.)
- bxn — Basalt NW of Whitehorse Bluff (m.? Pleist.)
- baw — Basaltic andesite W of Arant Point (m. Pleist.)
- bbi — Basaltic andesite W of Bear Bluff (m.? Pleist.)
- bcw — Basaltic andesite W of Mazama Campgr. (m.? Pleist.)
- bwc — Basaltic andesite of Whitehorse Creek (m.? Pleist.)
- acc* — Andesite N of Castle Creek (m. Pleist.)
- Basaltic andesite, undivided (Pleist. or Plio.)
  - b — Lava
  - bi — Intrusive
- bac — Basaltic andesite of Castle Point (e.? Pleist.)

Contact

Dike

Fault — Dottted where concealed; bar and ball on downthrown side

Volcanic vent — Does not include dikes feeding lava flows

244 ± 4 **Dated sample** — Location and age (ka) of sample dated by K-Ar or $^{40}Ar/^{39}Ar$ methods

MZI-11A **Geothermal exploration well**

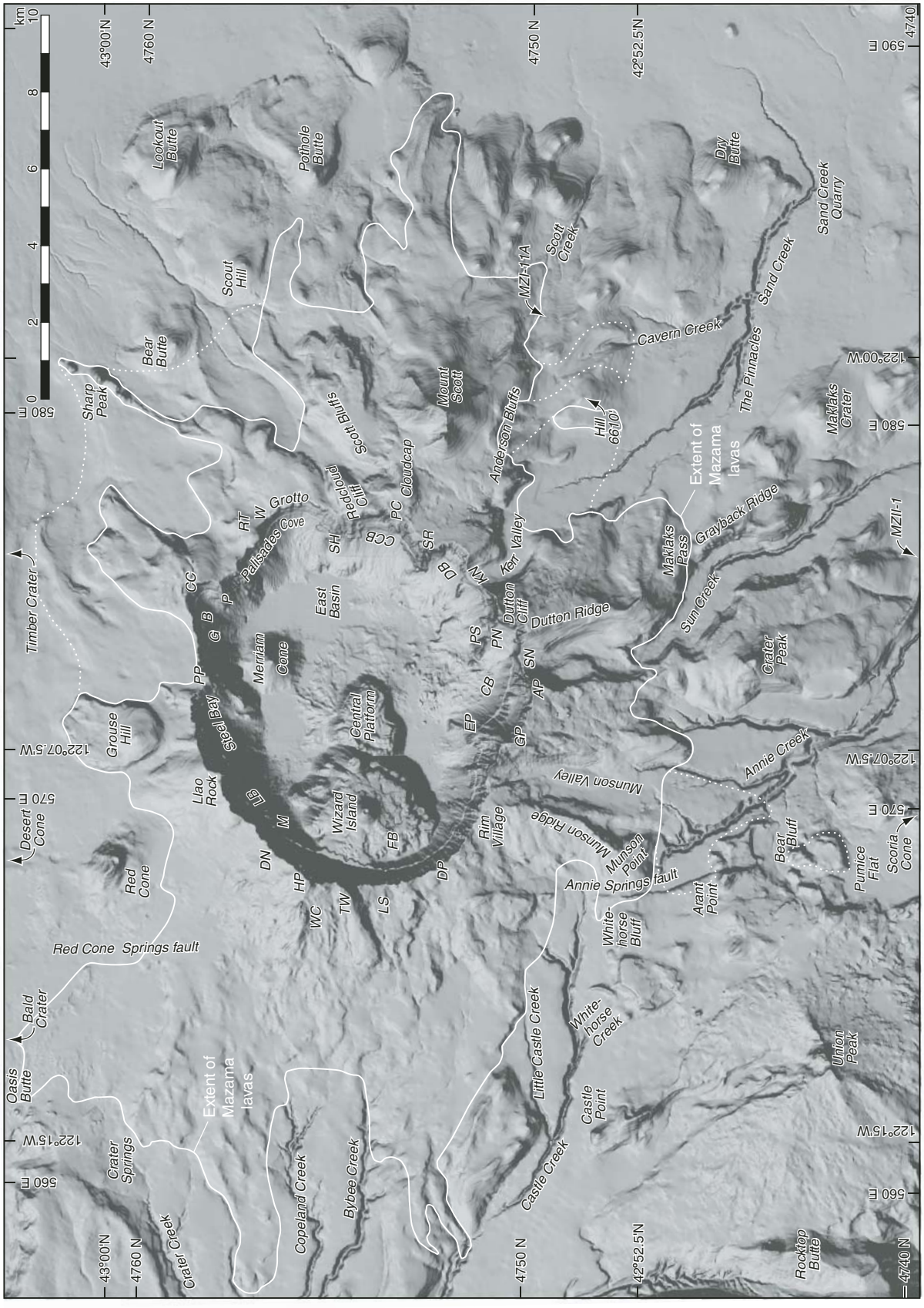

Figure 3. Shaded relief map of same area as Figure 2. Topography is from U.S. Geological Survey 10 m digital elevation model (DEM); bathymetry is from Gardner et al. (2001). White line indicates extent of Mazama lavas; dotted white line encloses additional possible areas. Place name abbreviations near and within Crater Lake caldera are: AP—Applegate Peak; B—Boat Landing; CB—Chaski Bay; CC—Cleetwood Cove; CCB—Cloudcap Bay; DB—Danger Bay; DN—Devils Backbone; DP—Discovery Point; FB—Fumarole Bay; G—Gauging station; GP—Garfield Peak; HP—Hillman Peak; KN—Kerr Notch; LS—Lightning Spring; LB—Llao Bay; M—Merriam Point; P—Palisade Point; PN—Phantom Cone; PS—Phantom Ship; PC—Pumice Castle; PP—Pumice Point; RT—Roundtop; SR—Sentinel Rock; SH—Skell Head; SN—Sun Notch; TW—The Watchman; WC—Williams Crater; W—Wineglass. MZI-11A and MZII-1 are geothermal exploration wells. Tick marks at edge of map are latitude, longitude, and UTM Zone 10 Eastings and Northings (km).

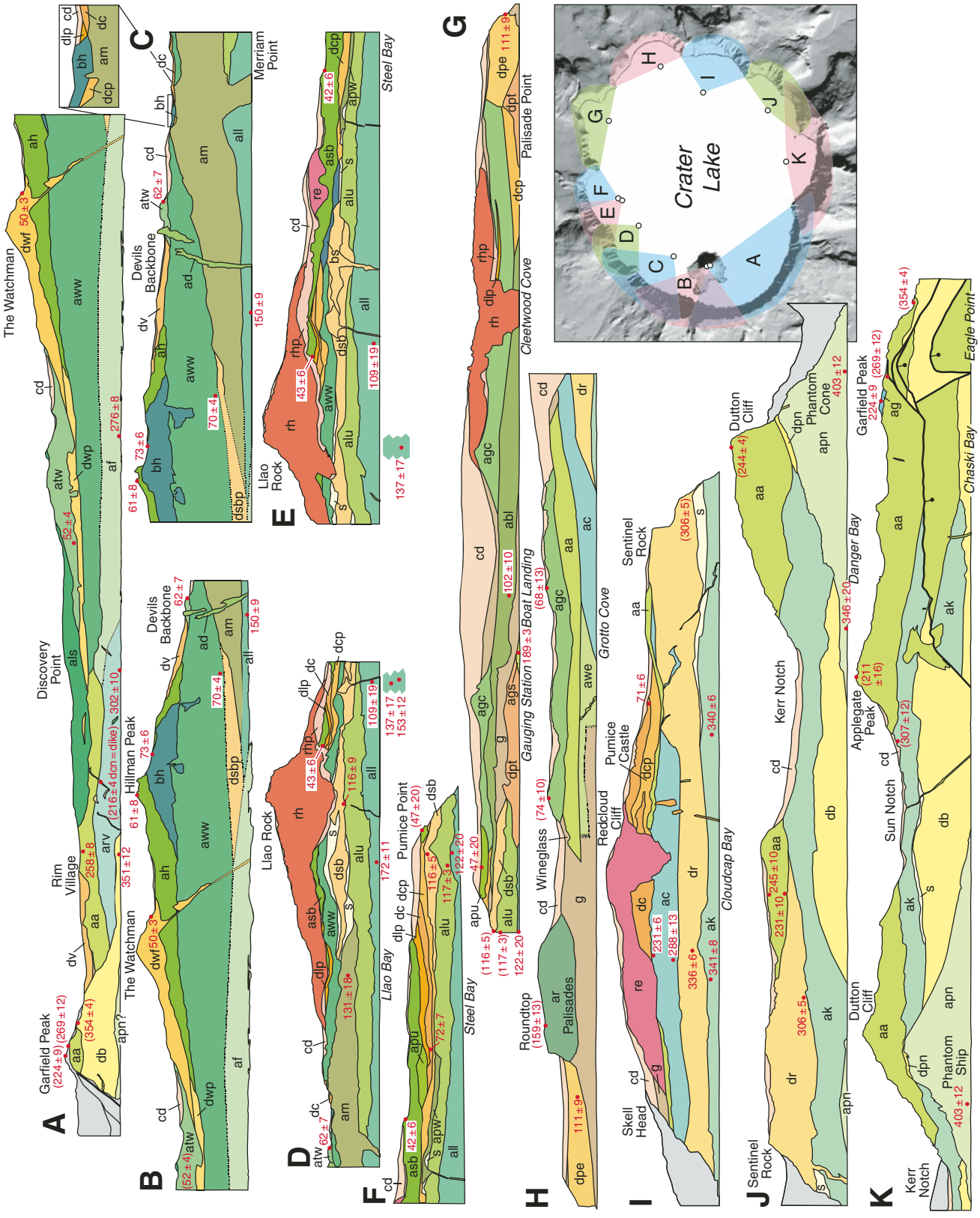

Figure 4. Geologic panoramas of the caldera walls, adapted from Bacon (2006) by inferring extent of map units beneath talus and vegetation. Unit cd represents climactic pumice fall, Wineglass Welded Tuff, lithic breccia, and ignimbrite of the climactic eruption. Explanation of units, etc., is as in Figure 2. Inset shows view points for each panorama. Scale varies because panoramas were plotted on photo mosaics. Note enlarged view of top of caldera wall in panorama C.

bedrock outcrops, a 1:50,000-scale interpretive bedrock geologic map, and detailed geologic panoramas with elevation contours appear in Bacon (2007).

Geologic Map Units

Map units represent products of an episode of eruptions from a source vent or, uncommonly, groups of coeval vents (e.g., units **bx, dc**). Such episodes may have lasted as little as a few months or as much as a few tens of thousands of years for some of the more extensive, older units. Map units typically are restricted in composition, but some have a range of compositions (e.g., unit **aa**). The principal features of a volcanic map unit are stratigraphic position and compositional kinship; phenocryst mode and texture must be consistent with the other criteria, as well as the mineralogy and composition of any microxenoliths (typically bits of holocrystalline gabbro or diorite), aggregates (crystal mush with intergranular melt), or enclaves (undercooled blobs of magma). Some older units are less restrictively defined than younger ones because of alteration of rocks low on the south caldera walls and (or) widely separated outcrops (e.g., unit **db**). Paleomagnetic pole positions were determined by D.E. Champion (2004, personal commun.) for many late Pleistocene units and all subaerial Holocene units. Paleomagnetic secular variation provides a key tool for temporal correlation of noncontiguous exposures and assignment to map units. More detailed descriptions of map units can be found in Bacon (2007).

Ar Geochronology

Most of the age determinations were by the K-Ar method (Table A1[1]), while 10 were from $^{40}Ar/^{39}Ar$ incremental heating experiments (Table A2, see footnote 1). Preferred ages for geologic units are given in Table 1. Analyzed materials were whole-rock samples crushed to 0.5–1 mm. For K-Ar geochronology, up to 25 g were fused for Ar analysis and 10 g were powdered for duplicate K_2O determinations by flame photometry on each of two splits. The Ar isotopic composition of the purified gas was measured on a multicollector mass spectrometer (Stacey et al., 1981). Reported errors for K-Ar ages are estimates of the standard deviation of analytical precision (±1σ). For samples with multiple Ar

[1]GSA Data Repository item 2006219, K-Ar and $^{40}Ar/^{39}Ar$ ages and analytical data and volume estimates for eruptive units, is available on the Web at http://www.geosociety.org/pubs/ft2006.htm. Requests may also be sent to editing@geosociety.org.

TABLE 1. PREFERRED K-Ar AND $^{40}Ar/^{39}Ar$ AGES, AGE RANGES, AND AGE ESTIMATES FOR MAP UNITS IN THE CRATER LAKE REGION

	Map label	Age type	Age or range (ka)
Regional volcanism			
Basaltic andesite north of Crater Creek	bck	KA	1879 ± 22
Basaltic andesite of Whitehorse Creek	bwci	KA	1379 ± 22
Andesite south of Dry Butte	adsi	WM	1088 ± 13
Andesite west of Sand Creek	asw	KA	670 ± 12
Basaltic andesite east of Annie Falls	baf	WM	651 ± 28
Andesite of Sun Creek valley	as	KA	623 ± 16
Basaltic andesite north of Lookout Butte	blp	KA	605 ± 25
Andesite north of Castle Creek	acc	KA	587 ± 18
Andesite northeast of Annie Falls	aaf	WM	517 ± 15
Andesite of Arant Point	at	WM	297 ± 12
Basaltic andesite of Maklaks Crater	bmc	KA	220 ± 67
Basaltic andesite of Whitehorse Bluff	bx	KA	217 ± 16
Basaltic andesite of Desert Cone	–	WM	213 ± 26
Basaltic andesite of Oasis Butte	bo	WM	201 ± 13
Basaltic andesite of Bald Crater	–	KA	192 ± 20
Basaltic andesite of Union Peak	bu	WM	164 ± 11
Andesite south of Lookout Butte	alb	KA	155 ± 6
Andesite of Timber Crater	atc	I	137 ±1 0
Basaltic andesite northwest of Pumice Flat	bf	KA	116 ± 24
Andesite of Crater Peak	acr	E	100–130
Andesite of Scott Creek	asc	I	87 ± 15
Basaltic andesite of Scoria Cone	bsc	P	53 ± 4
Basaltic andesite of Red Cone	br	P	35 ± 4
Pre-Mazama volcanics			
Dacite of Dry Butte	dd	WM	1275 ± 14
Dacite of Sand Creek	dsc	KA	1058 ± 16
Rhyodacite west of Cavern Creek	rcc	KA	724 ± 5
Dacite west of The Pinnacles	dw	KA	612 ± 8
Submerged caldera wall outcrops	su	KA	563 ± 20
Rhyodacite of Pothole Butte	rpb	E	410–460
Rhyodacite of Scott Creek	rsc	E	410–460
Mount Mazama ca. 420–180 ka			
Dacite of Mount Scott	ds	E	~420
Andesite of Phantom Cone	apn	WM	403 ± 12
Dacite of Chaski Bay	db	R	350–380
Andesite of Kerr Notch	ak	R	300–340
Dacite of Sentinel Rock	dr	E	300–340
Andesite below Rim Village	arv	KA	302 ± 10
Andesite west of Fumarole Bay	af	KA	276 ± 8
Dacite of Munson Ridge	dm	KA	276 ± 11
Andesite of Cloudcap Bay	ac	WM	287 ± 10
Andesite of Applegate Peak	aa	R	210–270
Andesite of Garfield Peak	ag	WM	224 ± 9
Dacite north of Castle Creek	dcn	WM	216 ± 4
Andesite of the gauging station	ags	P	189 ± 3
Mount Mazama ca. 180–80 ka			
Andesite east of Munson Valley	amv	KA	172 ± 15
Andesite of Llao Bay, lower unit	all	R	140–170
Andesite of Roundtop	ar	KA	159 ± 13
Andesite of Merriam Point	am	KA	131 ± 18
Andesite of Llao Bay, upper unit	alu	P	117 ± 3
Dacite of Steel Bay	dsb	WM	116 ± 5
Dacite east of Palisade Point	dpe	WM	111 ± 9
Andesite of the boat landing	abl	KA	102 ± 10
Mount Mazama ca. 80–40 ka			
Andesite west of Red Cone	arw	KA	84 ± 13
Andesite of the west wall	aww	WM	70 ± 4
Andesite of Grotto Cove	agc	WM	71 ± 5
Dacite of Pumice Castle	dc	WM	71 ± 5
Basaltic andesite of Hillman Peak	bhi	KA	73 ± 6
Andesite of Hillman Peak	ah	WM	61 ± 8
Andesite south of The Watchman	atw	WM	55 ± 3
Andesite of Devils Backbone	ad	E	40–50
Dacite of The Watchman	dwf	KA	50 ± 3
Andesite of Lightning Spring	als	WM	47 ± 8
Andesite of Pumice Point	apu	KA	47 ± 20
Andesite of Steel Bay	asb	WM	43 ± 4

Age type: KA—single K-Ar date; WM—weighted mean of at least two K-Ar dates; I—$^{40}Ar/^{39}Ar$ isochron; P—$^{40}Ar/^{39}Ar$ plateau; E—estimate based on K-Ar date(s); R—range based on K-Ar dates on two or more samples. Uncertainties are ±1σ.

analyses, weighted-mean ages are given where weighting is by the inverse of the variance of the individual measurements. Further details of K-Ar methods applied to young volcanic rocks by the USGS Menlo Park laboratory are given by Hildreth and Lanphere (1994).

Approximately 100 mg splits of the same material prepared for K-Ar dating were used in $^{40}Ar/^{39}Ar$ incremental heating experiments. Samples and fluence monitors were packaged in copper foil, placed in quartz vials, shielded in cadmium foil, and irradiated for 2 h in the USGS TRIGA reactor in Denver, Colorado. The resistance-heated furnace used for Ar extraction was attached to the cleanup system and mass spectrometer described by Dalrymple (1989). Plateau ages ($\pm 1\sigma$) were calculated for those gas fractions released contiguously that had ages in agreement within experimental error. Isochrons were fit to the data for plateau gas fractions. A detailed description of this $^{40}Ar/^{39}Ar$ dating protocol is presented by Lanphere (2000). For samples with both K-Ar and $^{40}Ar/^{39}Ar$ data, the two ages agree within error for fresh rocks with >1% radiogenic ^{40}Ar yield in the K-Ar procedure. For other samples, the $^{40}Ar/^{39}Ar$ result is preferred because of alteration or insufficient radiogenic ^{40}Ar yield.

Erupted Volumes

The interpretive bedrock geologic map was used to reconstruct approximate original extents and thicknesses of lava units in order to determine eruptive volumes. Caldera collapse provides a unique view of the internal structure of the volcano but requires speculation on the areal extent of many units, some of which are only known from caldera wall exposures. Volumes of such beheaded units were estimated by constructing in ArcInfo roughly elliptical polygons thought to outline their original extent, calculating areas, estimating minimum and maximum thicknesses, and assuming conical forms that of necessity ignored underlying topography. Errors in such reconstructions can be substantial. Changes in minimum thickness affect calculated volume considerably because these apply to the entire extent of the unit. Confidence is greatest in the volumes of younger units and least in relatively old units that are largely buried and have been most affected by glacial erosion. Volumes are quoted in the text to two significant figures, recognizing that this implies greater precision than commonly is warranted.

Volumes of Pleistocene pyroclastic units also had to be estimated from limited data. We constrained these volumes with available information on thicknesses and distributions, supplemented by analogies with historical eruptions of similar apparent magnitude. Likely errors are substantial but do not greatly affect overall conclusions because only the Holocene climactic eruption was of sufficient magnitude to dominate any part of the eruptive record. Volumes of Holocene pumice fall deposits were taken from Young (1990) and the climactic pyroclastic flows from Bacon (1983). Table A3 (see footnote 1) presents estimated volumes for all eruptive units.

The volume of reconstructed Mount Mazama was calculated using ArcInfo for comparison with the summed estimated volumes of relevant map units. Mount Mazama was approximated by constructing 100 m contours that represented the precollapse summit and the flanks as if they had not been glaciated. Elevation points were added to avoid clipping at the highest contours. The basal surface of Mazama was modeled by extrapolating the morphology of pre-Mazama units exposed on the periphery beneath the edifice. Basal and edifice surfaces were interpolated from the digital contours and elevation points. The difference between these surfaces gave a volume of reconstructed Mount Mazama of 112 km^3.

REGIONAL VOLCANISM

The Quaternary High Cascades at the latitude of Crater Lake are characterized by dominantly basaltic andesitic lava flows from isolated cinder cones (monogenetic volcanoes) and larger shield volcanoes (Bacon, 1990; Bacon et al., 1994). Andesites and true basalts are less common. Products of regional volcanism apparently underlie the entire map area, continue north and south, as well as interfinger with some distal Mazama lavas and overlie others.

Shield Volcanoes

Union Peak is the eroded feeder intrusion of an ~7-km-diameter shield volcano in the southwest corner of the geologic map (Figs. 2 and 5D). The volcano consists of ~6 km^3 of basaltic andesite (54%–56.5% SiO_2), typically with sparse olivine ± plagioclase phenocrysts and common polycrystalline aggregates; it mainly occurs as lava flows (unit **bu**) but also locally as cinders and palagonitic tuff on the shoulders of the central intrusion (**bui**). A glacial valley in the north flank exposes intrusive rock that probably was subjacent to early fissure vents. Lava high on the east flank yielded a weighted mean K-Ar age of 164 ± 11 ka. The palagonitic tuff probably reflects eruption during MIS 6 (Fig. 6). On the west, Union Peak lavas overlie an older, deeply eroded basaltic andesite shield (unit **b**) and its intrusive core (**bi**; Fig. 2).

The ~9 km^3 Timber Crater shield that lies mainly north of the map (Fig. 5D) evokes a less-eroded Union Peak volcano. Lava morphology is well preserved on the comparatively dry, lightly glaciated east flank. A flow on the southwest flank yielded only 0.4% radiogenic ^{40}Ar and a K-Ar age of 19 ± 19 ka. The same sample has a $^{40}Ar/^{39}Ar$ isochron age of 137 ± 10 ka, which is preferred over the 115 ± 4 ka plateau age because of the nonatmospheric $^{40}Ar/^{39}Ar$ intercept. Because no ice-contact features were found in a reconnaissance of the volcano, it seems likely that its age may be close to the minimum allowed by the $^{40}Ar/^{39}Ar$ isochron. Thus, the Timber Crater volcano escaped most or all of the MIS 6 glaciation, whereas the Union Peak volcano was present for at least the last ~30 k.y. of MIS 6 (Fig. 6). Timber Crater lavas (unit **atc**) are andesites (58%–59% SiO_2) that have olivine and plagioclase phenocrysts. The olivine in relatively phenocryst-rich samples has been resorbed and the plagioclase is joined by augite ± orthopyroxene. The presence of early crystallizing olivine in andesite suggests high pre-eruptive magmatic H_2O concentration (Sisson and Grove, 1993).

Monogenetic Vents

The regional monogenetic vent pattern in the Cascade arc is 30–40 km wide near Crater Lake. Over 40 source vents for monogenetic lavas have been identified within the area of Figure 2. Many vents that produced regional lavas form north-south alignments of similar age and composition and are the surface expression of dikes that propagated parallel to the maximum horizontal compressive stress. North-south–elongated intrusions are exposed at Rocktop Butte (**bi**), south of Highway 62 east of Whitehorse Creek (**bwc**), north of Union Peak (**bui**), and at Arant Point (**at**). Prominent vent alignments are delineated by Red Cone and a fissure system ~1.5 km to its north (**br**), several vents in a 6-km-long array south of Whitehorse Bluff (**bx**), and cinder cones and fissure vents west of Pumice Flat (**bf**) and of the Scoria Cone group (**bsc**; Scoria Cone itself is south of the map area).

Pre-Mazama Regional Lavas West of Crater Lake

Basaltic andesite lava flows of units **b**, **bac**, and **bck** make up forested mesas in the western part of Figure 2, west to the Rogue River, and also the eroded volcanic center west of Union Peak. Basaltic andesite north of Crater Creek (**bck**) yielded a K-Ar age of 1879 ± 22 ka. Farther east, finely porphyritic basaltic andesite of Whitehorse Creek (unit **bwc**; 53.5%–54.5% SiO_2) consists of lava flows, palagonitic tuff, and

Figure 5 (*on following three pages*). Geologic maps showing assembly of map in Figure 2 in six time increments. Areas of units have not been reconstructed; faults are omitted. Gray areas in panels B–F depict units emplaced in earlier time increments. Explanation of units, etc., is as in Figure 2. Present lake shoreline for reference is shown in blue. Dotted blue lines indicate vent alignments. (A) Units older than 350 ka. (B) 350–260 ka. (C) 260–180 ka. (D) 180–80 ka. (E) 80–40 ka. (F) 40–0 ka. Here unit cd represents thick climactic ring-vent-phase ignimbrite only. See Figure 3 for complete set of place names. Tick marks at edges of maps are latitude, longitude, and UTM Zone 10 Eastings and Northings (km).

an 800-m-long north-south–elongated intrusion. Lava flows that overlie unit **bac** on the Castle Point ridge, ~3.5 km west-southwest of the dike, are provisionally included in unit **bwc**. A sample of the **bwc** dike has a K-Ar age of 1379 ± 22 ka.

Sparsely porphyritic plagioclase + augite + orthopyroxene andesite lava flows (unit **acc;** ~0.3 km^3; 58.5% SiO_2) descending to Castle Creek near the western boundary of the park and on the ridge north of Little Castle and Castle Creeks can be traced southeast to an eroded cinder cone. The K-Ar age of 587 ± 18 ka is consistent with unit **acc** being overlain by **dcn** (216 ± 4 ka).

Pre-Mazama Regional Lavas South of Crater Lake

Four dated units are locally exposed at the bases of glacial valley walls south of Mount Mazama. Hydrothermally altered andesite west of Sand Creek (**asw**; 62.5% SiO_2) has a K-Ar age of 670 ± 12 ka that is consistent with its being overlain by units **rpb** and **aa**. Porphyritic andesite of Sun Creek (**as**; 62.5% SiO_2; K-Ar age 623 ± 16 ka) crops out beneath a thick unit **ak** flow at the head of the valley of Sun Creek. Sparsely olivine-phyric basaltic andesite east of Annie Falls (**baf**; 52.5% SiO_2; K-Ar age 651 ± 28 ka) is overlain by porphyritic andesite northeast of Annie Falls (**aaf**; 57.5% SiO_2; K-Ar age 517 ± 15 ka), and both are overlain by pre-Mazama rhyodacite lavas (**rcs),** the cliffs of which form the eastern wall of the valley of Annie Creek.

Pre-Mazama Monogenetic Vents East of Crater Lake

At least eight pre-Mazama monogenetic vents for basaltic andesite and andesite are preserved east of Mount Mazama within the area of Figure 2. An andesite plug (**adsi**; 57% SiO_2) south of Dry Butte is dated by K-Ar at 1088 ± 13 ka. Basaltic andesite of a cinder cone north of Lookout Butte (**blp**; 53% SiO_2) has a K-Ar age of 605 ± 25 ka. Other isolated, basaltic andesitic cinder cones and local lava flows are presumed to be middle Pleistocene, although some (e.g., **bap**, **bdp**, **bep**, **btp**) could be older.

A ca. 300 ka AndesiteTuya

Arant Point in the south-central part of the map is the heavily glaciated intrusive core of the cinder cone vent for andesitic lava (57%–58% SiO_2) of the adjacent tuya (Mathews, 1947; unit **at**; 0.14 km^3; Fig. 5B). Polygonal-jointed vitric andesite with sparse olivine and plagioclase phenocrysts is preserved in the intrusion margin and tuya carapace where lava contacted glacial ice or meltwater. A weighted-mean K-Ar age of 297 ± 12 ka is consistent with eruption during MIS 8 (Fig. 6). Arant Point is cut by the Annie Springs fault (Bacon et al., 1997b, 1999), which displaces unit **at** a maximum of 160 m down-to-the-east.

Basaltic Andesite ca. 220–190 ka

Several monogenetic vents were active between ca. 220 and ca. 190 ka (Fig. 5C). All produced basaltic andesite (53%–54% SiO_2) with olivine and plagioclase phenocrysts, and many sport polycrystalline aggregates or microxenoliths of olivine + plagioclase. In the southeast, Maklaks Crater cinder cone and its lava field (unit **bmc**; 0.45 km^3; K-Ar age 220 ± 67 ka) lie atop pre-Mazama rhyodacite. Lava from Desert Cone, north-northwest of Crater Lake (north of Figs. 2 and 5D), gave a weighted-mean K-Ar age of 213 ± 26 ka. A lava flow from Bald Crater, west of Desert Cone, has a K-Ar age of 192 ± 20 ka. The heavily glaciated Oasis Butte plug and a dissected cinder heap 1 km to its south mark vents for extensive lava (unit **bo**; 0.44 km^3; weighted-mean K-Ar age 201 ± 13 ka) in the northwest corner of the map with relatively coarse and abundant olivine accompanied by plagioclase and augite, as well as common microxenoliths of plagioclase + augite ± olivine or orthopyroxene.

Basaltic andesite of Whitehorse Bluff (unit **bx**; 1.4 km^3; 55–56.5% SiO_2) forms a tuya southwest of the caldera and includes lavas from four vents in a 6-km-long north-south array east of Union Peak (Fig. 5B). These phenocryst-poor lavas are distinguished by relatively high incompatible element concentrations (e.g., 1.3–1.4% K_2O, 800–1100 ppm Sr) and may include rocks of more than one age. A sample from west of Pumice Flat gave a K-Ar age of 217 ± 16 ka, which suggests that southern flows of this unit are younger than northern flows that are overlain by unit **dm** (see following). Sparsely porphyritic basaltic andesite west of Arant Point (unit **baw**; 0.16 km^3; 55.5–56% SiO_2; not dated) overlies northern flows of **bx**, also has high incompatible element concentrations, and underlies unit **at** (297 ± 12 ka). Thus, northern **bx** lavas probably are older than 300 ka.

Basaltic Andesite and Andesite ca. 160–100 ka

Three monogenetic vent areas are known from this interval (Fig. 5D). The oldest is porphyritic andesite lava (59% SiO_2; K-Ar age 155 ± 6 ka) that contains olivine + plagioclase + augite + orthopyroxene phenocrysts and ubiquitous plagioclase + augite ± orthopyroxene ± Fe-Ti oxide microxenoliths, and an associated cinder cone south of Lookout Butte (unit **alb**; 0.03 km^3) that rests on rhyodacite of Pothole Butte 10 km east-northeast of Crater Lake. Its disequilibrium phenocryst assemblage indicates that this andesite is a hybrid or contaminated.

Roughly 50 k.y. later, porphyritic andesite lava (unit **acr**; 0.66 km^3; 57%–58% SiO_2) issued from the base of the Crater Peak cinder cone 6 km south of Crater Lake and flowed in topographic depressions between three pre-Mazama rhyodacite units into Annie and Sun Creek valleys to at least ~8 km south of the vent. Rock and crystal compositions imply that the lavas are mixtures of mafic and dacitic magma ± plutonic rock (Bacon, 1990). Unit **acr** yielded K-Ar ages of 98 ± 8 ka and 136 ± 8 ka, which probably represent the same event sometime between ca. 100 and ca. 130 ka. Preservation of lava cascades at the margins of, and of flow remnants in, the deep glacial valleys of Annie and Sun Creeks is consistent with an age younger than MIS 6 (Fig. 6). Units **bcnp** (K-Ar age 207 ± 53 ka; thought to be too old owing to excess ^{40}Ar from rhyodacite xenoliths) and **bcsp** (K-Ar age 118 ± 48 ka) may represent the mafic end member (53.5% SiO_2) in unit **acr**. All three units would have been erupted during a short period along a north-south fissure system, with the relatively voluminous unit **acr** venting from a longer-lived central conduit. Eruption of hybrid andesite at Crater Peak would be consistent with lateral dikes emanating from the 100–120 ka active conduit of Mount Mazama. Thus, Crater Peak may be a satellitic vent of Mount Mazama rather than a monogenetic regional volcano.

West-southwest of Crater Peak, ~7–8 km, a 3-km-long north-south chain of plugs, dikes, and cinder exposures represents the glaciated

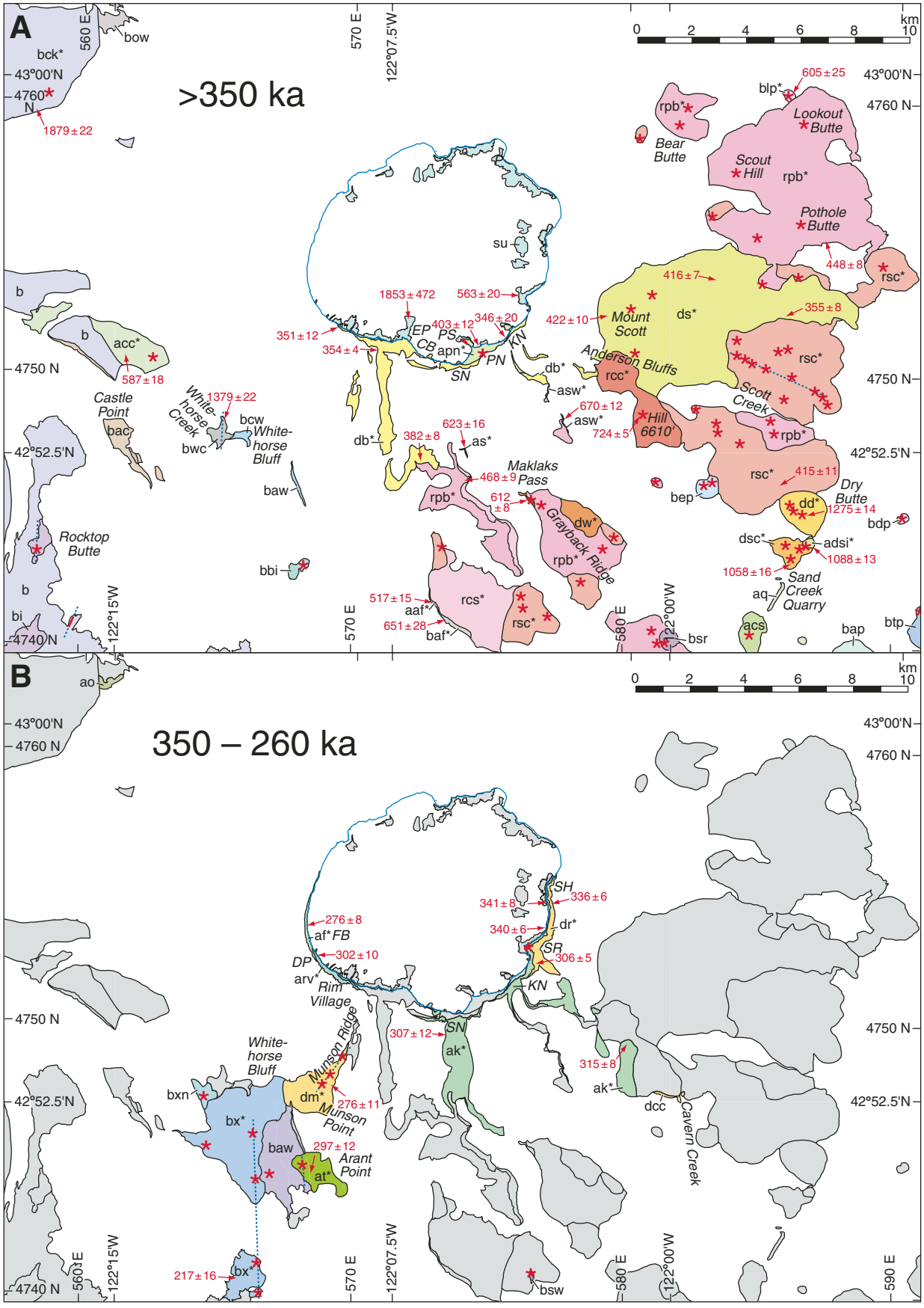

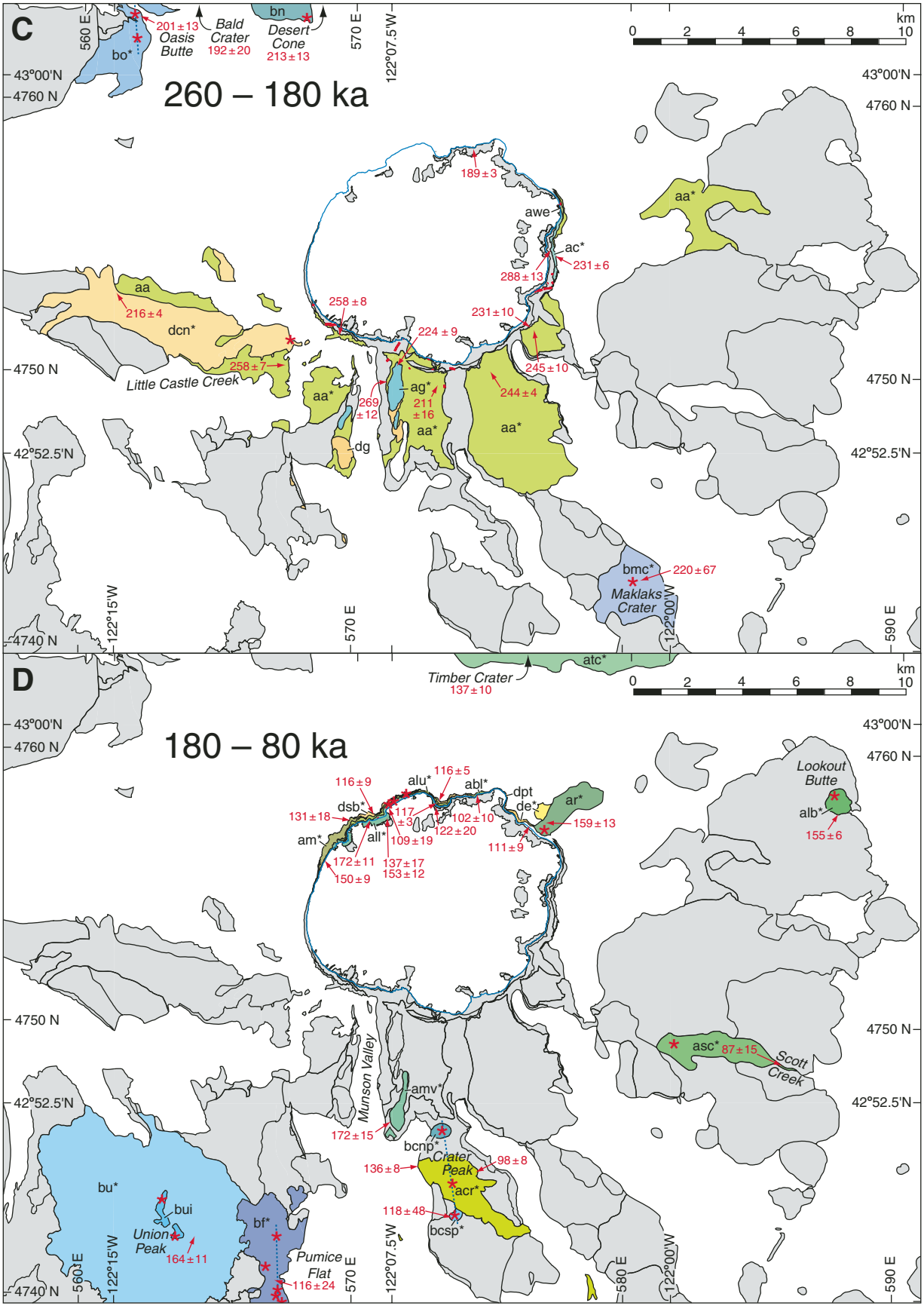

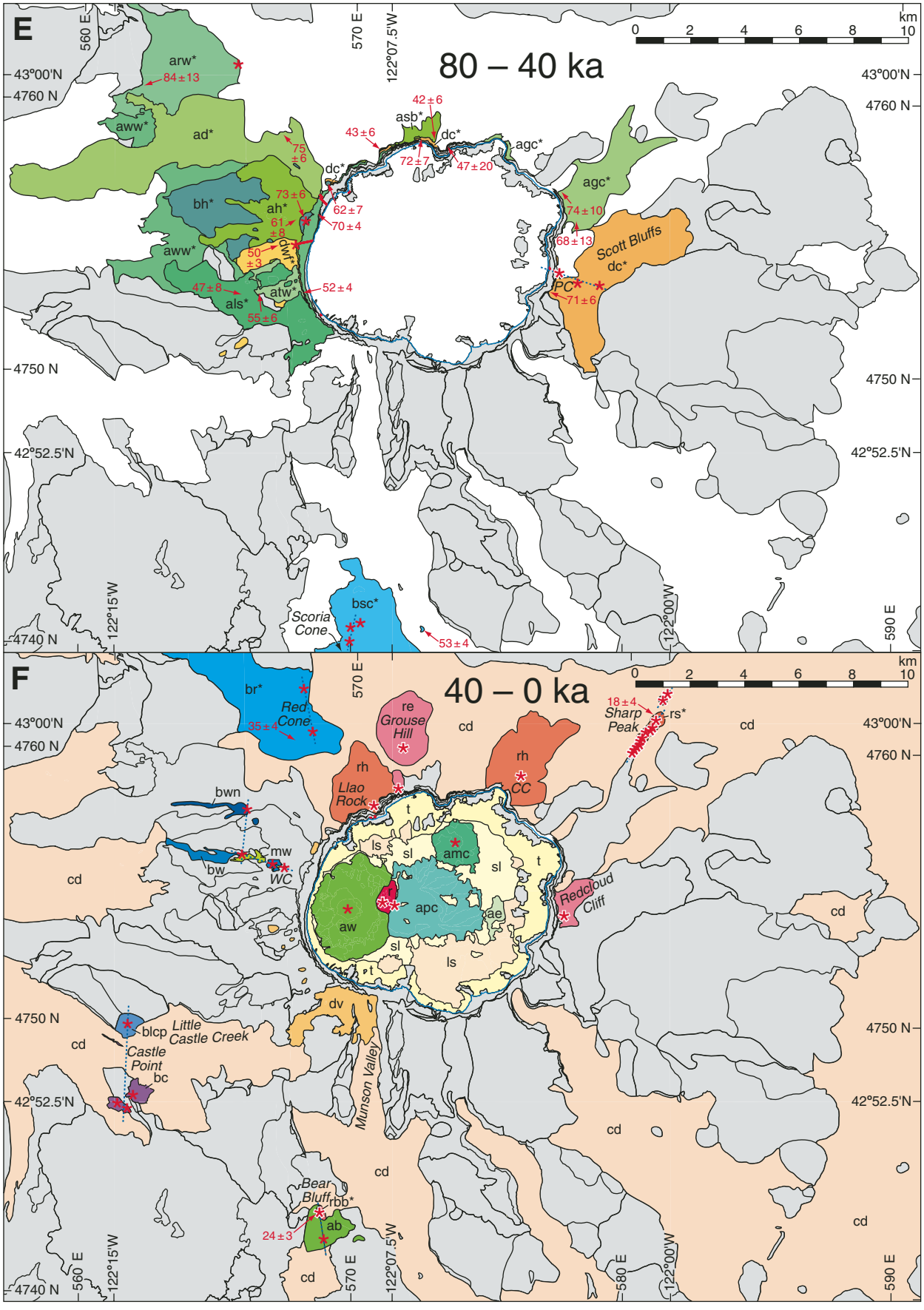

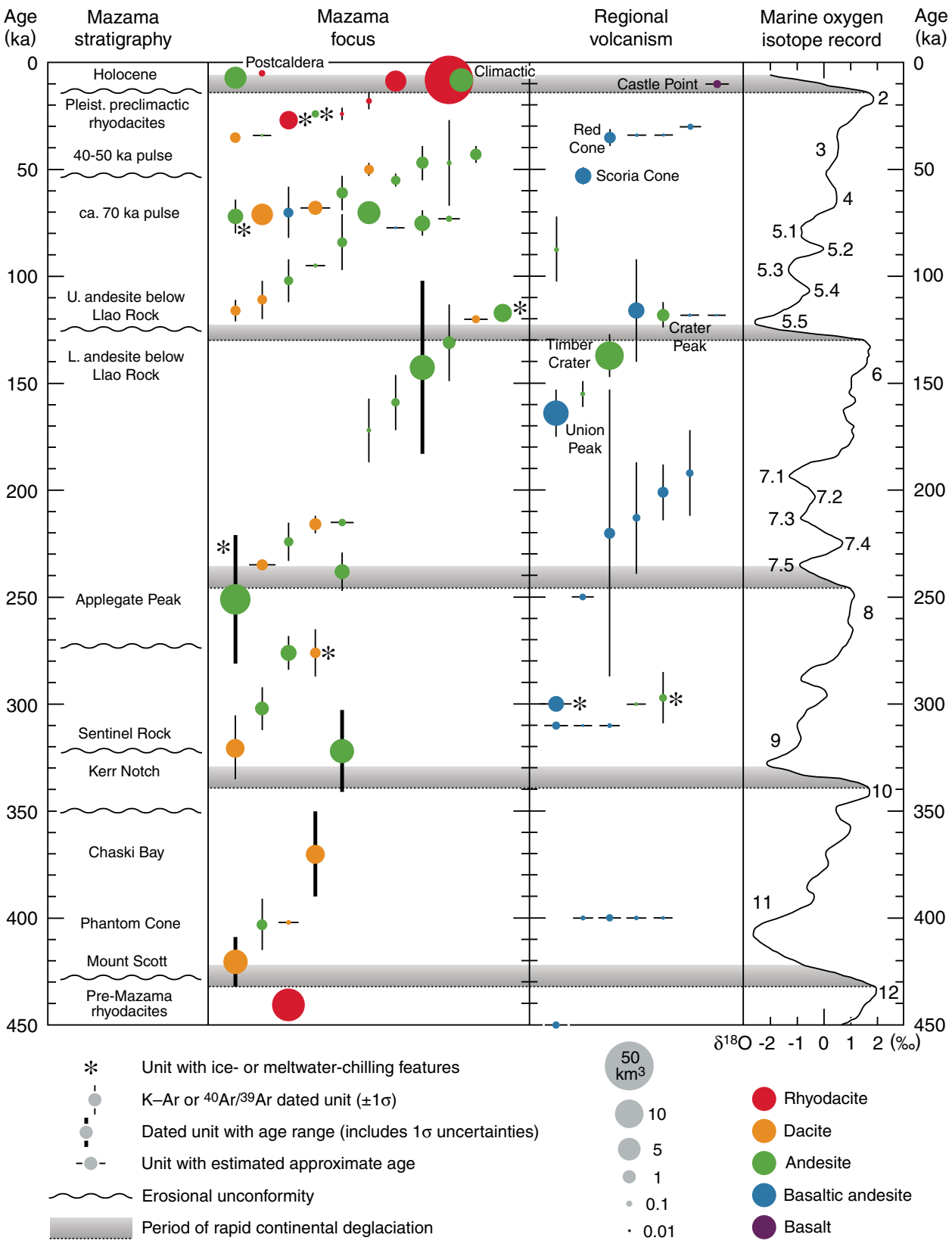

Figure 6. Generalized stratigraphic column for Crater Lake region showing K-Ar and $^{40}Ar/^{39}Ar$ ages, average compositions, and relative erupted magma volumes of units. Pre-Mazama rhyodacite (units rsc, rcs, rpb) are plotted at approximate age of 440 ka. Horizontal placement of unit symbols is arbitrary. Marine oxygen isotope (MIS) record (Bassinot et al., 1994; their Fig. 7), with selected numbered MIS, is at right for reference.

remnant of an eruptive fissure system bounding Pumice Flat on the west. These vents were active at approximately the same time as Crater Peak and produced sparsely phyric basaltic andesite (unit **bf**; 1.5 km^3; 55%–55.5% SiO_2) dated at 116 ± 24 ka. Common olivine + plagioclase microxenoliths distinguish this unit from its neighbors.

Andesite Vent Above Scott Creek

An eroded cinder cone 6 km southeast of the caldera is the source of porphyritic andesite lava that flowed into the Scott Creek drainage (**asc**; 0.07 km^3; 57.5%–59% SiO_2; Fig. 5D). A lava sample yielded only 0.2% radiogenic ^{40}Ar and a K-Ar age of 28 ± 30 ka. Presence of glacial till on the lava and incision of the intracanyon portion of the flow indicate eruption before the LGM, which is consistent with the $^{40}Ar/^{39}Ar$ isochron age of 87 ± 15 ka. Although this orphan unit might be considered a satellitic vent of Mount Mazama, it is assigned to regional volcanism because the lava is compositionally unlike any analyzed Mazama lavas.

Late Pleistocene Basalt and Basaltic Andesite (ca. 55–30 ka)

Scoria Cone (just south of map) and associated vents form a 1-km-long north-northeast alignment between Pumice Flat and Annie Creek that produced porphyritic basaltic andesite lava (unit **bsc**; 1.6 km^3; 54.5%–55% SiO_2; Fig. 5E); it has conspicuous microxenoliths (to 1 cm) of coarse blocky augite ± small olivine ± plagioclase. Unit **bsc** is offset down-to-the-east by the Sevenmile Creek fault, part of the West Klamath Lake fault zone (Bacon et al., 1997b, 1999). Basaltic andesite of Scoria Cone may be the most voluminous product of regional volcanism younger than 100 ka in age (Fig. 6). Its $^{40}Ar/^{39}Ar$ plateau age of 53 ± 4 ka is consistent with the unit's relatively minor glaciation.

A breached cinder cone on the north valley wall of Castle Creek near Little Castle Creek, 7 km west-southwest of the caldera, vented coarsely porphyritic basaltic andesite (unit **blcp**; 52.5% SiO_2; Fig. 5F) carrying abundant microxenoliths of plagioclase ± olivine ± augite. Preservation of the cone and tephra at the margin of a major glacial valley suggests eruption during the last interglacial.

Red Cone, 3.5 km northwest of the caldera, and a fissure vent system extending 1.7 km north are the source of porphyritic magnesian basaltic andesite lava (unit **br**; 0.5 km^3; 52.5%–54% SiO_2; Fig. 5F) that carries phenocrysts and microxenoliths of olivine ± augite ± plagioclase. Basaltic andesite of Red Cone flowed ≥6 km west-northwest, around the vent for unit **arw**, and is characterized by coarse (to 5 mm), blocky olivine phenocrysts. Olivine-phyric **br**, rich in incompatible elements, represents the arc end member among primitive mafic lavas in the Crater Lake region (Bacon et al., 1997a). Samples with abundant augite (1198, 1523) apparently contained inherited ^{40}Ar and did not yield geologically meaningful K-Ar ages. A sample (355) that contains only olivine phenocrysts gave a weighted-mean K-Ar age of 36 ± 12 ka and a $^{40}Ar/^{39}Ar$ plateau age of 35 ± 4 ka. A 35 ka age is consistent with moderate glaciation of Red Cone and its lava flows and with an unusual steep, northwesterly paleomagnetic direction similar to that of the dacite of Munson Valley (unit **dv**; D.E. Champion, 1999, personal commun.). Unit **br** is offset >11 m down-to-the-east by the Red Cone Springs fault (Bacon et al., 1999). Red Cone lava overlies middle Pleistocene(?) unit **bn** and high-alumina olivine tholeiite (48.5%, rarely to 50% SiO_2) lava flows from a vent 3.5 km east-northeast of Oasis Butte, north of the area of Figure 2.

A small cinder cone ~1 km west of Hillman Peak, formerly known as Forgotten Crater (Williams, 1942), has been named Williams Crater after volcanologist Howel Williams (Fig. 5F). The Williams Crater complex includes basaltic andesite contaminated with gabbro (resulting in bulk SiO_2 content of a basalt), dacite, and hybrid andesite (Bacon, 1990). The basaltic andesite (unit **bw**; 51.5% SiO_2) comprises the cinder cone, a lava flow locally exposed 1–4 km west of the cone and possibly vented from a fissure, and dense enclaves within overlying unit **mw** dacite and hybrid andesite. Ubiquitous in the basaltic andesite are gabbroic microxenoliths or aggregates (~2–10 mm) of various combinations of olivine, plagioclase, and augite. Although this composite unit is not dated, the smooth contact of **bw** tephra on ca. 35 ka unit **dv** (see Growth and Destruction of Dacite Domes ca. 35 ka) at the caldera wall south of Devils Backbone suggests a similar age. Remnants of porphyritic basaltic andesite (52.5% SiO_2) lava and a cinder cone marking its vent on the Red Cone Springs fault 2.6 km north-northwest of Williams Crater, which make up unit **bwn**, are compositionally and texturally similar to lava of unit **bw** (Bacon, 1990). Unit **bwn** has a degree of preservation and paleomagnetic direction similar to those of **bw** that suggest an age of ca. 35 ka.

Postglacial Basalt

Basalt of Castle Point (unit **bc**; >0.15 km^3; 47.5%–50% SiO_2; Fig. 5F) is the youngest precaldera mafic unit. Lava issued from three vents: (1) phenocryst-poor primitive high-alumina olivine tholeiite (<1% olivine) from a small shield at the west base of Castle Point, (2) porphyritic more-differentiated high-alumina olivine tholeiite from a prominent vent marked by cinders on Castle Point itself, and (3) a less conspicuous vent at the west base of Castle Point ridge, southeast of vent 1. Thin high-alumina olivine tholeiite flows exposed in Castle Creek near Little Castle Creek may belong to unit **bc** (Bacon, 1990; Bacon et al., 1994). Abundant microxenoliths (≤1 cm) of plagioclase + olivine ± augite are the source of many phenocrysts in porphyritic lavas. Unit **bc** is distinct from high-alumina olivine tholeiite flows west of the area of Figure 2 along the Rogue River near Farewell Bend, which may be ca. 1 Ma in age (K-Ar age 1.25 ± 0.11 Ma near Prospect; Fiebelkorn et al., 1982). Unit **bc** is postglacial because spatter ramparts and lava tubes near Castle Point are little modified, and because the basalt overlies LGM lateral moraines west and north of Castle Point and apparently overlies talus at vent 3.

PRE-MAZAMA SILICIC VOLCANICS

Domes and extensive lava flows of rhyodacite and dacite underlie Mount Mazama on its south and east (Figs. 2 and 5A). Nakada et al. (1994) assigned ~40 pre-Mazama rhyodacite lava flows and domes to three units (**rsc**, **rcs**, **rpb**) thought to have been emplaced over at most a few tens of thousands of years. A fourth rhyodacite and three dacite units southeast of Mount Mazama are significantly older.

Dacite

Dacite of Dry Butte (**dd**; 0.35 km^3; 63% SiO_2) has conspicuous hornblende phenocrysts + orthopyroxene + Fe-Ti oxides + abundant plagioclase and is the oldest silicic unit in the region (K-Ar age 1275 ± 14 ka). Although similar in appearance to pre-Mazama rhyodacites, the porphyritic dacite of Sand Creek (**dsc**; 0.1 km^3; 65.5%–68% SiO_2) is chemically distinct and much older (K-Ar age 1058 ± 16 ka). Field relations, K-Ar ages, and the composition of an enclave suggest that **dsc** may be coeval with the adjacent andesite plug **adsi** (1088 ± 13 ka). Rich in andesitic enclaves, porphyritic dacite west of The Pinnacles (**dw**; 0.3 km^3; 64%–65% SiO_2) that crops out on either side of Grayback Ridge is dated by K-Ar at 612 ± 8 ka. This unit is an excellent example of mingling (incomplete physical mixing) of silicic magma, gabbroic crystal mush, and undercooled basaltic andesitic magma (enclaves) where complex textures can be seen in outcrop. Porphyritic hornblende dacite (68% SiO_2), collected by submersible at 291 m depth off Sentinel Rock, predates Mount Mazama and gave a K-Ar age of 563 ± 20 ka.

Rhyodacite

Three closely related pre-Mazama rhyodacite units were defined by Nakada et al. (1994) on the basis of chemical composition and phenocryst content: rhyodacite of Scott Creek (**rsc**; 6.2 km^3; 68%–71.5% SiO_2), rhyodacite south of Crater Peak (**rcs**; 1.4 km^3; 71%–72% SiO_2), and rhyodacite of Pothole Butte (**rpb**; 5.6 km^3; 71.5%–73% SiO_2). Pre-Mazama rhyodacites are exposed beyond the limits of Mazama lavas from the East Fork of Annie Creek, counterclockwise to Bear Butte, ~3.5 km northeast of the caldera (Fig. 5A). A rhyodacite sample recovered by manned submersible off Palisade Point may be from a pre-Mazama flow. Nearly all the original pumiceous carapace has been removed from pre-Mazama rhyodacite lava flows. Domes north of Scott Creek, in the lee of Mount Scott, are the best preserved. Although commonly blanketed by Holocene pumice-fall deposits and (or) ignimbrite veneer, virtually every pre-Mazama rhyodacite hill is exposed on its caldera-facing summit because pyroclastic flows of the climactic eruption stripped the pumice-fall deposits and left insufficient veneer or lithic breccia to obscure the bedrock.

The three pre-Mazama rhyodacite units evidently are ca. 460–410 ka in age, but sparse whole-rock K-Ar dates are inconsistent with apparent stratigraphic relations. Paleomagnetic pole determinations by D.E. Champion (Nakada et al., 1994, their Fig. 5) support the distinction between units **rpb** and **rsc** and suggest that each unit erupted over a short interval. The age relation of **rpb** to **rsc** south of Scott Creek is ambiguous; elsewhere, **rpb** appears to be younger than **rsc**. Unit **rpb** has K-Ar ages of 468 ± 9 ka (west of Sun Creek) and 448 ± 8 ka (Pothole Butte), but a K-Ar age on the **rsc** flow north of Dry Butte is 415 ± 11 ka (although ages overlap at ±2σ). K-Ar ages of contiguous units suggest that the age of **rcs** is ca. 450 ka. Related pyroclastic deposits have been identified in three settings: (1) a ≥1-m-thick fall deposit is exposed beneath **rpb** basal vitrophyre where it lies on unit **dw** south of Maklaks Pass; (2) the MZI-11A geothermal exploration well ~4 km southeast of Mount Scott penetrated 123 m of rhyodacitic lava and 17 m of rhyodacitic(?) pyroclastics (Bacon and Nathenson, 1996); and (3) tephra layers above the Rockland ash bed in sediment cores, from Buck Lake and Wocus Marsh ~75 km south of Crater Lake and from Mohawk Lake in the northern Sierra Nevada, are compositionally similar to glass from units **rsc** and **rcs** (A.M. Sarna-Wojcicki, 2002, personal commun.). All of this is consistent with ages of ca. 450–550 ka. At present, evidence is lacking for voluminous pre-Mazama rhyodacitic pyroclastic-flow deposits or a buried caldera.

The rhyodacite west of Cavern Creek (**rcc**; 0.8 km^3) consists of felsite and rare obsidian of the poorly exposed lava dome of Hill 6610 (73% SiO_2) and altered porphyritic felsite of eastern Anderson Bluffs (72.5% SiO_2) south of Mount Scott. Unit **rcc** is older (K-Ar age of dome 724 ± 5 ka) and chemically more evolved than the three units that Nakada et al. (1994) grouped as pre-Mazama rhyodacite (**rsc**, **rcs**, **rpb**).

MOUNT MAZAMA

Mount Mazama was one of the major Cascade volcanoes before its collapse formed Crater Lake caldera. By projecting flank slopes upward, and through comparison with other volcanoes, Williams (1942) inferred a maximum elevation of ~3700 m. From the directions of glacier motion recorded by scratches on outcrops, Atwood (1935) showed that the summit of Mount Mazama was above the south-central part of Crater Lake. The caldera is thus eccentric to the Mazama edifice. The remains of Mount Mazama include the peaks outlining the caldera, the terrain sloping outward from them, and, 3 km east of the caldera, Mount Scott. Lavas and volcanic deposits of the contiguous edifice that are younger than the pre-Mazama rhyodacites (**rsc**, **rcs**, **rpb**) are assigned to Mount Mazama, although older andesite and dacite are known from limited manned submersible traverses of the drowned caldera walls and from the MZI-11A exploration well east of the park. Composed almost entirely of lava flows, the bulk of Mazama is andesite and low-silica dacite, while dacite and basaltic andesite are subordinate. Lavas of Mount Mazama are exposed in a crudely elliptical pattern with the major axis oriented east-west (Figs. 2 and 3). Most flows end within ~5 km of the caldera, but a few can be traced as far as 11 km. Like many other large, long-lived volcanoes, Mazama is made up of overlapping shields and stratovolcanoes, each of which probably was active for a comparatively brief interval. Erupted magmas had a range of parents characterized by varying isotopic compositions and incompatible element concentrations (Bacon et al., 1994). Ages and stratigraphic relations indicate that the focus of activity migrated from east to west (Fig. 5). Clearly, a volcanic center has been producing intermediate to silicic magmas in this location for a long time.

The superb exposures in the caldera walls and cliffs of glacial valleys provide cross-sectional and longitudinal views of lava flows and pyroclastic deposits that reveal that most of the lavas were fed from low fountains. Individual flow units grade from proximal bomb deposits through streaky lava to distal homogeneous, commonly flow-banded lava (e.g., units **aa** in Sun Notch and valley walls and **ds** on Mount Scott). Other examples are thin sheets of mafic andesite that may have great lateral extent (units **ac** and **all**). Lavas of Mount Mazama initially had rubbly tops that amounted to as much as half of the thickness of a flow. In the south caldera walls where hydrothermal alteration is most intense, rubbly flow tops appear yellowish because high primary permeability allowed relatively strong alteration to clays and minor pyrite and oxidation of pyrite colored the flow-top breccia. Bases of lava flows may be strikingly columnar jointed and vitric, especially where lava flowed over damp soil or till (e.g., **dr** above Danger Bay). A typical lava flow has a zone of subhorizontal platy joints above basal columns or breccia (e.g., **abl** on the trail above the Boat Landing). Above the plates may be a relatively massive core surmounted by more platy joints and, at the top, block-jointed lava grading up into flow-top rubble. Platy joints may wrap around the interior of a flow in onion-like fashion, so that the plates are steep at flow margins. Lava that erupted when ice was present displays ice-contact and water-chilling features, such as closely spaced vitric columns 10–20 cm in cross section (polygonal joints; Lescinsky and Fink, 2000; Smellie, 2000), which are often of sizeable thicknesses and which may grade up into vitric breccia (e.g., unit **aa** on Dutton and Grayback Ridges and at Wineglass; **alu** near Pumice Point).

Unlike many large composite volcanoes, Mount Mazama evidently did not have an abundance of pyroclastic flowage deposits or an apron of lahars about its base prior to the climactic eruption. The near absence of exposed volcanic fragmental deposits probably is a result of late Pleistocene flushing of drainages and burial by climactic ignimbrite. Pyroclastic-flow or hot volcanic avalanche deposits, such as those which form by collapse of lava domes or steep-fronted flows, are represented only in units **dr** and **dv**. The only other mappable pumiceous pyroclastic-flow and pyroclastic-fall deposits that are part of Mazama itself are ca. 70–50 ka dacite units **dcp**, **dlp**, and **dwp**.

Many dikes are visible in the caldera walls. Several can be traced into lava flows (Fig. 4) or correlate with lava on the flanks of Mount Mazama. The dikes commonly have glassy selvages with horizontal columnar joints. Irregular intrusions are present below Hillman and Applegate Peaks and in Phantom Cone (named by Williams, 1942; Figs. 4B, 4C, and 4K).

Early Mount Mazama (older than 350 ka)

Dacite of Mount Scott

Mount Scott was the principal vent for a great pile of porphyritic dacite (unit **ds**; 5.5 km^3; 63.5%–67% SiO_2; most ≥65%; Fig. 5A) that grades from pyroclastic breccia and agglutinate sheets proximally to massive lava distally and is everywhere characterized by basaltic andesitic enclaves (≤50 cm; 53.5%–56.5% SiO_2). The greatest enclave concentration is on the southeast ridge of Mount Scott, in which enclaves are virtually touching, suggesting ejection as rigid clasts in eruptive fountains and accumulation in near-vent agglutinate, followed by flowage. Flank vents are present on the northeast and at Anderson Bluffs. Like those of many other andesites and dacites of Mount Mazama, **ds** textures result from mixtures of silicic melt, undercooled enclave material, cumulate crystal mush, and gabbroic microxenoliths. Typical **ds** lava contains a total of 25%–30% phenocrysts of plagioclase (≤5 mm; commonly coarsely sieved, blocky crystals and crystal fragments), augite (≤1.2 mm, rarely to 5 mm), orthopyroxene (≤1.2 mm), and Fe-Ti oxides (≤0.2 mm) in a glassy to very fine-grained groundmass. Enclave fragments and kindred small crystals are ubiquitous. Many of the abundant microxenoliths and crystal aggregates (≤8 mm) contain olivine (typically ≤1.5 mm, rarely to 4 mm). The lava is intensely altered locally to residual silica + minor specular hematite; clinopyroxene + K-feldspar are present in vugs and fractures and replace groundmass low in the northwest cirque. Dacite of Mount Scott yielded K-Ar ages of 422 ± 10 ka (west side of cirque) and 416 ± 7 ka (east flank). Lava included in unit **ds**, which possibly erupted from a flank vent and extending 8 km east of Mount Scott over pre-Mazama rhyodacites, gave a K-Ar age of 355 ± 8 ka; if accurate, this result implies a remarkable duration for eruption of similar dacite from the Mount Scott center.

Andesite and Dacite of Phantom Cone

The andesite of Phantom Cone (**apn**; 0.4 km^3; 60.5–61.5, rarely 63.5% SiO_2) consists of gently dipping lava flows, indurated near-vent fall deposits, and intrusions that make up Phantom Cone (Williams, 1942) in the southeast caldera wall (Figs. 4J, 4K, and 5A). Basaltic andesitic enclaves to 1 m are present in intrusive rock and are smaller in lava flows. The unit is capped by a distinctive quartz-bearing lava flow (dacite of Phantom Cone, **dpn**; 66% SiO_2) that also is found in the west wall of upper Kerr Valley; resorbed quartz xenocrysts (≤1 mm) are unique to **dpn**. Hydrothermal alteration is ubiquitous. Phantom Ship island is composed of resistant, altered **apn** lava flows with local cavities lined by drusy quartz; a northwest-trending dike is evident below lake level (Bacon et al., 2002). Dates for overlying units suggest that the K-Ar age of 403 ± 12 ka southeast of Phantom Ship is more accurate than that of 346 ± 20 ka at Kerr Notch.

Dacite of Chaski Bay

Porphyritic dacite of Chaski Bay lava flows and breccias (**db**; 2.5 km^3; 59.5%–67% SiO_2; mainly low-silica dacite) crop out at the edges of Kerr and Munson Valleys and low in the south caldera wall (Fig. 5A). Andesitic enclaves to 50 cm are common. Near the caldera, unit **db** is hydrothermally altered. K-Ar ages are 382 ± 8 ka (east fork of Annie Creek) and 351 ± 12 ka (below Rim Village). A $^{40}Ar/^{39}Ar$ plateau age of 354 ± 4 ka is considered more reliable than the K-Ar age of 333 ± 6 ka for a sample from below Garfield Peak. Unit **db** lavas probably span the range of ca. 350–380 ka.

Andesite and Dacite ca. 350–260 ka

Andesite of Kerr Notch

Remnants of a >8-km-diameter shield volcano are composed of thin flows that consist of variably porphyritic andesite of Kerr Notch (**ak**; 5.4 km^3; 59%–66% SiO_2; most 60%–63%). Unit **ak** lavas also floor Sun Notch, are found in the caldera wall from Grotto Cove to below Applegate Peak (Figs. 4H–K), and extend 5 km from the caldera in Sun Creek and Kerr valleys (Fig. 5B). Enclaves to 15 cm, enclave fragments, and plagioclase + pyroxene aggregates to ~5 mm are present in some flows. Alteration, restricted to the vicinity of the caldera, is less intense than in underlying units. Unit **ak** is distinguished from contiguous units **db** and **aa** by smaller and fewer phenocrysts and the presence of andesites with abundant plagioclase ≤0.4 mm; **ak** is separated from these units by erosion surfaces and sedimentary deposits or paleosols. K-Ar ages of 341 ± 8 ka and 340 ± 6 ka at Cloudcap Bay, 315 ± 8 ka east of Sand Creek, 307 ± 12 ka in Sun Creek valley, and 306 ± 7 ka ($^{40}Ar/^{39}Ar$ plateau age 303 ± 3 ka) for a lithic block in the **asc** cinder cone southeast of Mount Scott indicate an age range of ca. 340–300 ka.

Older Andesites of the Southwest Caldera Wall

The andesite below Rim Village (**arv**) and andesite west of Fumarole Bay (**af**) (Figs. 4A and 5B) had sources northwest of Garfield Peak. Porphyritic lavas of unit **arv** (0.9 km^3?; 59%–62% SiO_2) form the lower part of the caldera wall between Rim Village and Discovery Point. Large phenocrysts, an apparently separate population of microphenocrysts (≤0.3 mm), and common hornblende characterize most flows mapped as **arv**. Near lake level, below Discovery Point, the K-Ar age is 302 ± 10 ka. Radiating small glassy columns in the basal **arv** outcrop suggest contact with ice on the underlying **db** lava (glaciated at the end of MIS 10), which is consistent with the 302 ka age near the onset of MIS 8. Finely porphyritic unit **af** lava flows (1.5 km^3?; 61.5%–62% SiO_2) crop out low in the caldera wall between Discovery Point and The Watchman. Lava at lake level has a K-Ar age of 276 ± 8 ka.

Dacite of Sentinel Rock

Fed by a dike, porphyritic dacite of Sentinel Rock (**dr**; 2.4 km^3?; 63%–65.5% SiO_2) is exposed widely in the caldera wall (Figs. 4H–J and 5B), fills a glacial valley cut in unit **ak** south of Sentinel Rock, and lies on glaciated **ak** near Skell Head. Glaciation of unit **ak** is inferred to have occurred during the final ice advance in MIS 10. One of the few block-and-ash-flow deposits of the Mazama edifice forms the lower half of unit **dr** ~500 m south of Skell Head. Common basaltic andesitic enclaves (55.5%–56.5% SiO_2) carry gabbroic aggregates and microxenoliths. K-Ar ages on the lowest lava flows are 306 ± 5 ka south of Sentinel Rock and 336 ± 6 ka at Cloudcap Bay.

Andesite of Cloudcap Bay

The relatively mafic, moderately porphyritic andesite of Cloudcap Bay (**ac**; 1.2 km^3; 55.5%–60% SiO_2; most >57%) forms many thin, extensive agglutinate sheets (Figs. 4H, 4I, and 5B). Presence of dikes (57.5%–61% SiO_2) and oxidized scoria indicate a source vent above Cloudcap Bay. The lowest flow at Cloudcap Bay gave a K-Ar age of 288 ± 13 ka. Two K-Ar analyses of the highest flow there yielded 219 ± 7 ka and 285 ± 15 ka; because there is no evidence for significant pauses during accumulation of the lava flows, we consider the 285 ± 15 ka age to be the more accurate. If so, the entire unit was erupted within the resolution of the two older, indistinguishable K-Ar ages, which have a weighted mean of 287 ± 10 ka.

Dacite of Munson Ridge

Thick dacitic lava (unit **dm**; 0.4 km^3; 64.5%–65% SiO_2) separates the drainages of present-day Castle Creek and Munson Valley on the southwest flank of Mount Mazama (Fig. 5B). Vitric breccia and columns on the lava surface indicate flow beneath ice. Joint and flow-banding patterns, and relatively abundant enclaves, suggest a vent beneath Munson Point; other vents or eruptive fissures may be present beneath Munson Ridge, fed by a radial dike system from Mazama. Phenocrysts in the porphyritic dacite apparently

were derived from olivine gabbro microxenoliths (≤7 mm) and crystal mush (typically <1 cm, rarely to 15 cm with 56.5% SiO_2). Uncommon andesitic enclaves (58.5%–59.5% SiO_2) to 15 cm contain rare 1 mm olivine. Unit **dm** has a K-Ar age of 276 ± 11 ka (MIS 8.4) and is cut by the north-south Annie Spring normal fault.

Andesite and Dacite ca. 260–180 ka

Voluminous Andesite of Applegate Peak

Like other large Cascade volcanoes (e.g., Mount Adams, Hildreth and Lanphere, 1994; Mount Baker, Hildreth et al., 2003a), Mount Mazama had episodes of rapid cone building. The most obvious of these produced the andesite of Applegate Peak (unit **aa**; 11 km^3; 57%–66.5% SiO_2), a compositionally diverse pile of fountain-fed lava flows that erupted principally from the summit vent between ca. 270 and ca. 210 ka (mainly 250–230 ka). Applegate Peak, Dutton Cliff, and the upper south slopes of Mount Mazama are composed of this unit. The most extensive unit of Mount Mazama, unit **aa** lava is exposed in the upper half of the caldera wall from Wineglass clockwise to Discovery Point (Figs. 4A and 4H–K) and as far from the caldera as 9 km east near Scout Hill, 5 km south at Maklaks Pass, and 8 km west in Bybee Creek (Figs. 2 and 5C). Andesite of Applegate Peak forms dikes in the caldera wall at Grotto Cove, Cloudcap Bay, Sun Notch, and Chaski Bay, and on the Garfield Peak trail at 7650 ft elevation, as well as a large intrusive body in the caldera wall below Applegate Peak (Figs. 4A and 4H–K). Ice was present during much of this episode near the end of MIS 8, as shown by columnar (polygonal) joints and breccias such as at Wineglass, high on Dutton Ridge, northwest of Maklaks Pass, and along Rim Drive southeast of Kerr Notch. The distribution of **aa** with ice-contact jointing indicates that glaciers occupied the major valleys radiating from Mount Mazama and implies that the edifice approached its maximum height at that time. Doubtless, lava that flowed onto the major glaciers broke up and was transported great distances as lahars, which have been scoured away by ice and streams or buried beneath climactic ignimbrite.

Andesite of Applegate Peak typically contains 20%–30% of phenocrysts dominated by plagioclase, commonly in two populations—one that is coarsely sieved and resorbed, and the second, less abundant, one that is finely sieved, has clear overgrowths, and is accompanied by augite, orthopyroxene, and Fe-Ti oxide. Characteristic plagioclase laths (≤0.3 mm, ≤15%) contrast with a very fine-grained or glassy groundmass. Olivine xenocrysts (≤2 mm) are typically rimmed by basaltic andesitic groundmass. The most mafic flows have as little as 7% total phenocrysts of plagioclase, augite, and olivine in a groundmass rich in plagioclase laths. Enclave fragments and medium-grained crystal aggregates (to ~1 cm) are common, giving unit **aa** lava a similar appearance to unit **db**, but the abundance of enclaves smaller than a few centimeters typically is lower. Andesitic enclaves (55%–58% SiO_2) as much as 20 cm across are present in many unit **aa** flows. Many phenocrysts were derived from crystal aggregates; plagioclase laths <1 mm long may have originated in enclave magma. The varied lava composition results in part from dacitic magma mixing with basaltic andesitic magma (e.g., thin flows east of Garfield Peak); at least two basaltic andesite components are indicated by the range in incompatible element concentrations. Seven K-Ar ages range from 269 ± 12 ka to 211 ± 16 ka (Table A1, see footnote 1). Unit **aa** flows were glaciated before being overridden by lava of slightly younger units **ag** (224 ± 9 ka) south of Garfield Peak and **dcn** (216 ± 4 ka) north of Little Castle Creek.

A kindred porphyritic dacite flow, which erupted from a satellite vent 1 km south of Garfield Peak (unit **dg**; 0.5 km^3; 64.5%–65.5% SiO_2; andesitic enclaves to 50 cm near vent), is present nearly 6 km from its source where it is displaced by the Annie Spring fault ~2 km southeast of Arant Point. Unit **dg** is younger than **aa** below Garfield Peak (K-Ar age: 269 ± 12 ka) but older than **ag**.

Andesite of Garfield Peak

This moderately porphyritic hornblende (≤3 mm) andesite (**ag**; 0.27 km^3; 60.5%–61.5% SiO_2) consists of lava flows and breccia at Garfield Peak, on the slope to the south, and on the west side of Munson Valley (Fig. 5C). Fresh **ag** lava has a sharp basal contact with underlying, altered unit **aa** south of Garfield Peak. The K-Ar age of the highest flow on Garfield Peak is 224 ± 9 ka.

Extensive Dacite North of Castle Creek

A flank vent 2 km west of Rim Village produced uniquely Ti-rich, variably porphyritic dacitic lava that flowed due west for at least 10 km, forming the present divide between Bybee Creek and Castle Creek drainages, before it descended into both canyons (Figs. 2 and 5C). This dacite north of Castle Creek (**dcn**; 0.6 km^3; 64.5%–66.5% SiO_2) originated beneath Mazama, because dikes of identical composition (65%–66% SiO_2) in the caldera wall northwest of Rim Village (Fig. 4A) trend toward the mapped vent. The magma apparently broke through to the surface when lateral feeder dikes intersected the Annie Spring fault, which now displaces vent agglutinate. North of Castle Creek, unit **dcn** lies on **aa** lava (nearest dated sample 258 ± 7 ka), which apparently was glaciated in MIS 7.4 or possibly 8.0. A sample from the Bybee Creek drainage has a K-Ar age of 216 ± 4 ka.

Andesite of the Gauging Station

A porphyritic andesite lava flow (**ags**; 60% SiO_2) forms a glaciated promontory overlain by till at the gauge on the north shore of Crater Lake and small outcrops to its west (Fig. 4G). The andesite has a $^{40}Ar/^{39}Ar$ plateau age of 189 ± 3 ka and resembles some lavas of unit **aa**, but is ~20 k.y. younger than the youngest dated **aa** lava. The **ags** outcrops are the oldest lava above lake level for nearly half the circumference of the caldera, from Wineglass west to Fumarole Bay.

Andesite and Dacite ca. 180–80 ka

Andesite East of Munson Valley and at Llao Bay

Porphyritic andesite lava flows (**amv**; 0.02 km^3; 57% SiO_2), characterized by abundant seriate olivine, cap the ridge between the Middle and East Forks of Annie Creek 2–4.5 km south of Garfield Peak (Fig. 5D). A single K-Ar determination gave an age of 172 ± 15 ka.

About the same time that unit **amv** was erupted, different andesitic magma began to construct a large shield on the northwest flank of Mazama. The shield grew in two episodes (units **all** and **alu**, Figs. 4B–4G) spanning ca. 170 to 120 ka; an unconformity separates the two packages of similar, fountain-fed sheets of relatively mafic andesite.

Variably porphyritic andesite lava flows of the lower unit (**all**; 6 km^3?; 57%–60.5% SiO_2) crop out in the caldera wall from south of Devils Backbone to east of Pumice Point. These lavas commonly show patchy groundmass alteration to clay minerals and amygdules containing clay ± carbonate minerals. Six K-Ar ages range from 172 ± 11 to 109 ± 19 ka (Table A1, see footnote 1). Alteration of some samples and a $^{40}Ar/^{39}Ar$ age of overlying unit **alu** imply that the age of **all** is ca. 170–140 ka.

The upper unit of the andesite of Llao Bay consists of variably porphyritic basaltic andesite and andesite lava flows (**alu**; 2.2 km^3?; 54.5%–61% SiO_2) in the caldera wall from Merriam Point to east of Pumice Point. Lavas are altered to varying degrees west of Steel Bay. Lava at Pumice Point has been dated by K-Ar at 106 ± 7 ka and by a $^{40}Ar/^{39}Ar$ plateau at 117 ± 3 ka. The latter age is consistent with K-Ar ages of contiguous units. The dated flow has closely spaced columnar joints that grade into vitric breccia at Pumice Point, where it lies on glaciated flows of unit **all** (Fig. 4F). Although glaciation of the **all** lava could have occurred near

the end of MIS 6, the ice-contact and meltwater chilling features in the **alu** lava probably date from MIS 5.4.

Andesite of Roundtop

The Palisades on the northeast caldera rim (Fig. 4H) consist of porphyritic andesite of Roundtop (**ar**; 0.18 km^3; 62% SiO_2), a single lava flow that extends 2.5 km northeast (Fig. 5D; not to be confused with the Palisade dacite flow of Williams, 1942). The joint pattern in the cliffs suggests that the vent lies beneath Roundtop. Resting on 115 m of glacial deposits, **ar** lava is probably an ice-bounded flow (Lescinsky and Sisson, 1998). The texture is typical of Mazama intermediate-composition rocks, and basaltic andesitic enclaves (to 20 cm) are common. Andesite of Roundtop has a K-Ar age of 159 ± 13 ka, solidly within MIS 6.

Andesite of Merriam Point

Porphyritic andesite of Merriam Point (**am**; 0.7 km^3?; 60.5%–61.5% SiO_2) forms a mound of thick flows in the northwest caldera wall from below Hillman Peak to below Llao Rock (Figs. 4B–4D). The unit is thickest (~250 m) above its feeder, which displaced and tilted unit **all** southwest of Merriam Point. Unit **am** is characterized by sharply euhedral, blocky plagioclase, commonly in stellate clusters, and it is relatively poor in incompatible elements (e.g., 0.8%–1.2% K_2O). It is separated from underlying **alu** by a clastic deposit and from overlying **dsb** by indurated bedded mudflow(?) deposits (unit **s**), and it is glaciated where overlain by **dc**. The K-Ar age is 131 ± 18 ka.

Other Lavas of the North Caldera Wall

Several andesite and dacite units, emplaced mainly as thick lava flows ca. 120–100 ka, are present in the caldera wall but are not exposed on the north flank of Mount Mazama. Connecting dikes (Fig. 4E) show that at least some of these units (**dsb, apw**) erupted from flank vents.

Dacite of Palisade Point (not dated), which is composed of enclave-bearing (to 30 cm) porphyritic lava at Palisade Point and east of Pumice Point (**dpt**; 0.16 km^3?; 66% SiO_2; Fig. 4G), overlies unit **all** (122 ± 20 ka, east of Pumice Point) and till (**g**), and is overlain by **alu** (117 ± 3 ka). The stratigraphically higher dacite of Steel Bay (**dsb**; 0.35 km^3?; 64.5%–66.5% SiO_2) locally rests on fluvioglacial sediments deposited on **alu** lava. A correlative pyroclastic-flow deposit containing hornblende-dacite (64.5% SiO_2) prismatically jointed blocks lies on **am** lava below Hillman Peak (Fig. 4B). Two prominent dikes feed a small dome and a lava flow of **dsb** at Steel Bay (Fig. 4E). Andesitic enclaves (≤1 m; 57.5%–59% SiO_2) are uncommon except near Pumice Point and in the eastern dike. Unit **dsb** has K-Ar ages of 116 ± 9 ka below Llao Rock and 116 ± 5 ka at Pumice Point.

The Palisade flow of Williams (1942), ~150 m thick, forms the northeast caldera wall between Palisade Point and Roundtop. This porphyritic dacite flow is here termed the dacite east of Palisade Point (**dpe**; 0.30 km^3?; 65% SiO_2; Figs. 4G and 4H). Enclaves (≤30 cm) are relatively abundant. The flow overlies unit **dpt** and probable till, apparently is banked against **ar**, and is overlain by till and **agc**. Bacon (1983, p. 82) suggested a 26–22 ka age on the basis of a radiocarbon date on the underlying paleosol (evidently contaminated with modern carbon) and provisional identification (incorrect) of underlying tephra. The K-Ar age of 111 ± 9 ka is consistent with stratigraphic relations.

Andesite of the boat landing consists of porphyritic lava flows and an underlying fragmental deposit between Pumice Point and Cleetwood Cove (**abl**; 0.24 km^3?; 63%–63.5% SiO_2; Fig. 4G). Andesitic enclaves (≤30 cm; 57.5% SiO_2), most common in the upper flow, contain olivine phenocrysts (≤2.5 mm). The trail to the boat landing descends along the base of the lower flow, dated by K-Ar at 102 ± 10 ka, where it lies on thick till laid down in MIS 5.4 and possibly 6.

The Big Pulse ca. 80–40 ka

Far-Traveled Western Andesites

Beginning ca. 75 ka, from a source west of the center of the present caldera, andesite of the west wall (**aww**; 4.6 km^3; 57%–61% SiO_2) spread as relatively thin lava flows that formed a 300-m-thick pile below Hillman Peak and extended from Steel Bay to below Discovery Point (Figs. 4A–E) and at least 7 km west in Bybee Creek (Fig. 5E). Distinguishing characteristics are seriate texture, common olivine, and, in most samples, relatively small pyroxene phenocrysts. East of Llao Rock, this unit includes two thick lava flows that are petrographically and compositionally similar to (older) unit **ar** and are overlain by a thinner flow of typical **aww** lava. Caldera wall exposures are altered below The Watchman and Hillman Peak. Andesite of the west wall is similar in age, texture, and composition to unit **arw**, mapped separately because of different source vents and because **arw** flows are overlain by finer-grained and more olivine-rich **aww** flows ~2 km southeast of Crater Springs. The latter **aww** flows apparently originated at a flank vent, ~2.5 km southeast of Crater Springs, presumably fed by a radial dike and subsequently buried by unit **ad** flows. The voluminous **aww** pile, dated by K-Ar at 70 ± 4 ka, is separated from older units **am** and **dsb** by a paleosol or by fragmental deposits, respectively.

Finely porphyritic seriate-textured andesite lava flows, which are exposed west of the Red Cone Springs fault as far west as Oasis Butte and ~1 km south of Crater Springs in the northwest part of Figures 2 and 5E, are assigned to the andesite west of Red Cone (**arw**; 0.3 km^3; 59% SiO_2). Their source vent apparently was ~2 km west of Red Cone, ~7 km north-northwest of the inferred principal source of **aww**. The **arw** vent probably was fed by a dike from the same magma reservoir beneath Mount Mazama that produced **aww** and that intersected the Red Cone Springs fault. The K-Ar age of an **arw** flow, 84 ± 13 ka, is nominally older but analytically indistinguishable from that of unit **aww**.

Devils Backbone is a prominent segmented dike cutting the entire caldera wall north of Hillman Peak. Moderately porphyritic andesite lava flows, from a vent fed by the Devils Backbone dike and since removed by glaciation, are included in the andesite of Devils Backbone (**ad**; 1.4 km^3; 57.5%–61% SiO_2; most 60%–61%). Unit **ad** extends 11 km west from the caldera rim. Characteristic blocky plagioclase and pyroxene (~0.1–0.4 mm) in a very fine-grained groundmass give the rock a seriate appearance and a crystal content of ~30%. Ubiquitous enclave fragments (≤5 mm) are rich in olivine (~1–3 mm). Gabbro and troctolite xenoliths as large as 1 cm are common. Devils Backbone dike cuts units **all**, **am**, **aww**, and **atw**, and **ad** lava overlies **aww**, **bh**, and **ah**. If correlation of dated lava with Devils Backbone dike and lava outcrops near the caldera rim is correct, the K-Ar age of 75 ± 6 ka from ~4.5 km northwest of Devils Backbone may be too old, possibly owing to abundant augite-bearing gabbro microxenoliths, and the eruption age may be 50–40 ka.

Small-Volume Lava Units at Steel Bay

Olivine-phyric basaltic andesite of Steel Bay (**bs**; 0.003 km^3?; 53% SiO_2) erupted from a nearby vent and deposited palagonitic tuff breccia and thin flows of the most mafic lava known in the caldera walls (Fig. 4E). Evidence for explosive interaction with water suggests that this unit (not dated) erupted during a wet period following emplacement of unit **aww**. Nearby andesite west of Pumice Point (**apw**; 0.01 km^3?) consists of porphyritic lava flows (61% SiO_2) and a feeder dike (59.5% SiO_2) at Steel Bay (Figs. 4E and 4F). Unit **apw** (not dated) overlies unit **alu** and is overlain by **dcp**. Units **bs** and **apw** are thought to be ca. 70–80 ka in age.

Voluminous Dacite of Pumice Castle and Kin

By ca. 70 ka, Mazama volcanism had changed character dramatically, producing voluminous dacite from several vents that extended

from Cloudcap 8 km west-northwest across the north side of Mount Mazama, and suggesting the presence of a large magma body. Dacite of Pumice Castle (66%–68% SiO_2) occurs as pyroclastic deposits (**dcp**) and lava flows (**dc**). Dikes and welded pumice-fall deposits north of Pumice Castle mark a major vent area (Fig. 4I). Lava issued from vents east of the caldera and flowed to either side of Mount Scott to form uppermost Anderson Bluffs and the coulees east of Scott Bluffs (Fig. 5E). Similar dacite lava occurs at Steel Bay and above Merriam Point and in a probable dike sampled by manned submersible below Llao Rock. The Plinian fall is a 75-m-thick deposit of alternating welded and nonwelded layers at Pumice Castle and nonwelded fall, pyroclastic-flow, or reworked deposits exposed locally from north of Devils Backbone to Palisade Point and above the Cloudcap Road. The Plinian fall was correlated by Davis (1985) with Summer Lake (Oregon) tephra bed 6 and by Rieck et al. (1992) with a 6-cm-thick ash layer at 16.99 m depth in Tulelake (California) core 1, indicating extensive downwind deposition. The correlative ash bed in the Tulelake core is ~20 cm below a paleomagnetic excursion, thought by Rieck et al. (1992) to be the Blake event but that may be in fact the Norwegian Sea event (D.E. Champion, 2005, personal commun.), which is considered to have occurred ca. 70 ka at the MIS 4–5 boundary (Bleil and Gard, 1989). Dacite of Pumice Castle represents the most voluminous silicic eruptions at Mazama between ca. 400 ka and the onset of rhyodacitic volcanism ca. 27 ka. The lava (**dc**) volume is ~1.8 km^3, and the pyroclastic (**dcp**) magma volume is estimated at 2 km^3. The unit is characterized by large, blocky augite (≤1.5 mm, rarely to 6 mm), which is more abundant than the generally smaller and ubiquitous gabbroic crystal aggregates (typically ≤8 mm). The K-Ar age of **dc** lava at Steel Bay is 72 ± 7 ka. Two K-Ar analyses on unit **dc** lava above Pumice Castle yielded 47 ± 12 ka and 71 ± 6 ka; the younger age is considered inaccurate because it is inconsistent with stratigraphic relations. Unit **dc** lava rests on **aww** flows (70 ± 4 ka nearby), and **dcp** pumice fall underlies a unit **bh** flow (73 ± 6 ka nearby) north of Devils Backbone (Fig. 4C). Our best estimate of the age of this important unit is the weighted mean of the two older age determinations on **dc** lava, 71 ± 5 ka.

Immediately above unit **dc** lava at Steel Bay is a pumice-fall deposit that is locally welded, indicating a nearby vent. This occurrence and related fall and pyroclastic-flow deposits in the caldera walls from north of Devils Backbone to Palisade Point (Figs. 4C–G) are termed dacite below Llao Rock (**dlp**; 66%–67.5% SiO_2); these have been correlated by Davis (1985) with Summer Lake (Oregon) tephra bed 8 and with ash at Lake Malheur, Oregon, on the Snake River in western Idaho, and at Butte Valley, California (A.M. Sarna-Wojcicki, 2002, personal commun.). Rieck et al. (1992) provisionally correlated a 3-cm-thick ash layer at 17.01 m in Tulelake core 1 with **dlp,** but this correlation is inconsistent with the order of the two ash layers in the core, i.e., the putative correlatives of **dcp** and **dlp** are stratigraphically reversed. The erupted magma volume is estimated to be ≥1 km^3. This porphyritic dacite pumice is distinguished from **dcp** by generally smaller plagioclase and augite, subequal proportions of augite and orthopyroxene, and less differentiated glass composition. Unit **dlp** overlies units **dc**, **aww**, **bh**, and **am**, is intercalated within **agc** at Cleetwood Cove, and is overlain by **apu** and **asb**. Its age probably is ca. 70 ka.

Basaltic Andesite of Hillman Peak

Distinctive hornblende-phyric basaltic andesite of Hillman Peak (**bh**; 0.32 km^3; 55.5%–59% SiO_2) vented where intrusions and near-vent fall deposits are exposed in the caldera wall (Figs. 4B and 4C), notably west of the summit of Mount Mazama, and lava spread west for at least 5 km (Fig. 5E). Some activity took place between the two voluminous dacitic pyroclastic eruptions, because at the northernmost caldera rim, **bh** lava lies on **dcp** fall and has **dlp** pyroclastic flow banked against it (Fig. 4C, inset). Samples of this unit have the highest incompatible element concentrations (e.g., 2.0% K_2O, 2000 ppm Sr) and most radiogenic Sr (Bacon et al., 1994) of any from the Mazama edifice. They carry a total of 20%–30% phenocrysts of plagioclase (<2 mm, rarely to 4 mm), hornblende (≤4 mm, rarely to 1 cm), and augite (≤3 mm), with or without orthopyroxene (≤1 mm) or Fe-Ti oxide (≤0.2 mm). Rare olivine (≤3 mm) is present in some samples and is intergrown with hornblende in one example. Aggregates and microxenoliths (≤4 mm, rarely to 1 cm) of plagioclase + augite ± orthopyroxene ± hornblende ± oxide are common. A sample from north of Hillman Peak has a K-Ar age of 73 ± 6 ka.

Ice-Bounded Andesite of Grotto Cove

Andesite of Grotto Cove (**agc**; 1.3 km^3; 61.5%–63% SiO_2) forms two 100-m-thick flows that traveled 3 km beyond the caldera rim (Figs. 4H and 5E). Joint patterns suggest that the flows banked against ice near the present caldera rim and that vents were near the southern limit of each flow. Like unit **ar**, these flows probably were ice-bounded. Other lava flows assigned to unit **agc** occur in the caldera wall from Pumice Point to Cleetwood Cove (Fig. 4G). The porphyritic lava is texturally similar to others at Mazama and contains aggregates (≤5 mm) of plagioclase + augite + orthopyroxene ± Fe-Ti oxide ± olivine. Andesitic enclaves, locally common between Pumice Point and Cleetwood Cove (≤40 cm; 58.5% SiO_2), contain crystal aggregates and phenocrysts of the same phases as in the host rock. Enclaves are abundant (5%–10%) near tops of flows at Grotto Cove, where the larger enclaves (12–100 cm) have porous diktytaxitic cores and 2–6-cm-thick denser rinds. Intergranular melt was expelled from enclave cores at Grotto Cove by gas-driven filter pressing (Bacon, 1986; Sisson and Bacon, 1999) that caused initially andesitic enclaves (60% SiO_2) to develop relatively mafic cores (≥55.5% SiO_2). The order of eruption appears to have been from most to least silicic lavas, starting at Cleetwood Cove and ending with the southern flow at Grotto Cove. K-Ar ages are 74 ± 10 ka for the northern flow at Grotto Cove and 68 ± 13 ka for the southern, stratigraphically higher flow. Paleomagnetic data suggest that the flows at Grotto Cove erupted over a period of ~100–200 yr (D.E. Champion, 1984, personal commun.). The weighted-mean age of 71 ± 5 ka is consistent with eruption during MIS 4.

Andesite of Hillman Peak

Distinctively porphyritic andesite lava flows (**ah**; 0.51 km^3; 57.5%–59% SiO_2) from a vent east of Hillman Peak form its summit, are exposed in the caldera walls (Figs. 4B and 4C), and extend 4 km down the west flank of Mount Mazama (Fig. 5E). The andesite has a speckled texture of abundant euhedral plagioclase (typically ~1 mm) accompanied by relatively large augite (to 4 mm) phenocrysts. Lavas of unit **ah** have unusually high incompatible element concentrations (Bacon et al., 1994). The K-Ar age of lava at Hillman Peak is 61 ± 8 ka.

Dacite of the Watchman

The Watchman dacite flow (Williams, 1942; unit **dwf**) is prominent on the west rim of Crater Lake caldera. Its feeder dike is obvious on the caldera wall. The Watchman is a glaciated horn above the vent for the 2-km-long lava flow (Figs. 4A, 4B, and 5E). Earlier lava, exposed in the caldera wall and west of Rim Drive, flowed an equal distance to the south. Nonwelded pumiceous pyroclastic-flow deposits (**dwp**) of an early phase of the eruption are present in rare patches on the Castle Creek–Bybee Creek divide ~4 km west of Rim Village and in the caldera wall in a paleovalley in unit **aww** that was glaciated during MIS 4. Pyroclastic-flow deposits probably were extensive in the Bybee and, possibly, Castle Creek drainages. The total magmatic volume is conservatively estimated at 0.3 km^3, but the pyroclastic component may

be underestimated. No fall deposit has been recognized, although pumiceous clasts above unit **dlp** at Palisade Point may correlate with **dwp**. The porphyritic dacite (65.5%–68% SiO_2; most ≥67%) is petrographically like other intermediate to silicic rocks of Mount Mazama, with the addition of rare hornblende (≤0.7 mm). Andesitic enclaves (61%–61.5% SiO_2; ≤15 cm) are rare. The north-south Annie Spring normal fault offsets the base of the platy jointed zone in **dwf** a minimum of ~15 m, down-to-the-east, 750 m west of Discovery Point. Dacite of the Watchman has a K-Ar age of 50 ± 3 ka.

Andesite South of the Watchman

Thick lava flows of andesite south of The Watchman (**atw**; 0.27 km^3; 62.5%–63.5% SiO_2) overlie unit **dwp** (Figs. 4A and 5E) and are cut by the Devils Backbone dike (Fig. 4C) at the caldera rim, suggesting a source between Hillman Peak and the Mazama summit. The coarsely porphyritic silicic andesite contains sparse enclaves and abundant aggregates (typically ~3 mm but commonly to 1 cm) of plagioclase ± olivine + augite ± orthopyroxene ± oxides + glass (devitrified) cumulate mush. Glassy columns at some exposures suggest chilling against ice (e.g., 2 km southwest of The Watchman). K-Ar ages of 62 ± 7 ka north of Devils Backbone, 55 ± 6 ka west of Lightning Spring, and 52 ± 4 ka south of The Watchman, have a weighted mean of 55 ± 3 ka. A far more voluminous outpouring of porphyritic andesite (**ad**) next took place from a vent or vents fed by the Devils Backbone dike (see *Far-Traveled Western Andesites* above).

Youngest Mazama Andesites

Andesites of Lightning Spring, Pumice Point, and Steel Bay are the youngest precaldera andesitic lavas known on Mount Mazama. They probably originated at or west of the summit ca. 50–40 ka. Porphyritic andesite of Lightning Spring (**als**; 0.64 km^3; 61.5%–65.5% SiO_2; most <64%) lava flows are present at the caldera rim from west of Rim Village northwest to the Lightning Spring trailhead and as far as 5 km from the caldera in the Bybee Creek drainage. A dike near lake level below Discovery Point is mapped as unit **als** (Fig. 4A). Pumiceous pillow-like **als** blocks (to ~1.5 m) are overlain by till 1.3 km west of Discovery Point as though lava flowed in a meltwater channel beneath ice; alternatively, the blocks are cauliflower bombs in a volcanic flowage deposit. Gabbroic aggregates and microxenoliths (≤5 mm, rarely to 1.2 cm) are ubiquitous, and many phenocrysts appear to be derived from these materials. Hornfels xenoliths (~1–2 cm, rarely to 20 cm) are locally present. Enclaves (≤6 cm, rarely to 40 cm) are rare. Unit **dwp** is intercalated within the lowest **als** flows in the caldera wall. The K-Ar age of an **als** sample is 47 ± 8 ka.

Present locally above Steel Bay and filling a paleovalley in unit **dcp** at Pumice Point (Figs. 4F and 4G), andesite of Pumice Point (**apu**; 0.03 km^3; 59.5%–61% SiO_2) is distinguished by its comparatively low phenocryst content (~3%–7%), presence of olivine, and distinctive groundmass texture. Its K-Ar age is 47 ± 20 ka at Pumice Point. The more porphyritic (~25% phenocrysts) andesite of Steel Bay lava flows (**asb**; 0.52 km^3; 59%–61% SiO_2) are present between Llao Bay and Steel Bay (Figs. 4D–F) and locally north of the caldera (Fig. 5E). Unit **asb** is the youngest precaldera andesite preserved, and it yielded K-Ar ages of 42 ± 6 ka and 43 ± 6 ka.

Growth and Destruction of Dacite Domes ca. 35 ka

The youngest dacites of the Mount Mazama edifice, both ca. 35 ka, are the dacite of Munson Valley (**dv**) and the dacitic component of the mingled lava of Williams Crater (**mw**; Fig. 5F). In addition to the usual phases, some samples contain sparse hornblende. Unit **dv** (0.4 km^3) consists of avalanche deposits, including block-and-ash flows, fed by collapse of lava dome(s) or steep flow front(s) high on Mount Mazama. The vent must have been immediately southwest of the summit, because these deposits are found only on the southwest flank and just south of Devils Backbone. Andesitic enclaves (≤20 cm; 60% SiO_2; Bacon, 1986) are common in the porphyritic dacite clasts (63.5%–69.5% SiO_2; most <65%). Textures and bulk compositions indicate that typical dacite of Munson Valley is a mixture of andesitic enclave magma and a dacitic end member containing crystal aggregates. Preservation commonly restricted to lees of topographic highs and rare striae on large clasts indicate that unit **dv** was glaciated. Although **dv** has not been dated, prismatically jointed blocks record an unusual paleomagnetic pole similar to that of unit **br** (D.E. Champion, 1999, personal commun.), which has a $^{40}Ar/^{39}Ar$ plateau age of 35 ± 4 ka.

Williams Crater is a basaltic andesitic cinder cone just west of the caldera rim on the shoulder of Hillman Peak. Similar gabbro-contaminated basaltic andesite forms a lava flow 1–4 km west of the cone [unit **bw**; see *Late Pleistocene Basalt and Basaltic Andesite (ca. 55–30 ka)*]. Mingled dacite and hybrid-andesite lavas (**mw**; 0.003 km^3; 60.5%–67% SiO_2) form a small dome immediately west of Rim Drive, two small lava flows at the south and east summits of the cinder cone, and a lava flow extending 1.2 km west from the cone. Vents define a N75°W trend, radial to the caldera. Gabbroic microxenoliths and dense enclaves of **bw** magma (to 2 m) are present in **mw** lavas. All but the most silicic layers in **mw** lavas are hybrid mixtures of dacite and gabbro-contaminated basaltic andesite. Superposition of unit **mw** on **bw** and **bw** bombs cored with angular blocks of **mw** indicate the following sequence of events (Bacon, 1990), which took place in a short interval constrained by identical paleomagnetic directions of both units and by Mg-Fe diffusion profiles in olivine (McKnight and Bacon, 1992): (1) entrainment of gabbroic crystal mush within basaltic andesite magma (**bw**); (2) intersection of a basaltic andesite dike with the west margin of a dacitic magma reservoir and dispersal of gabbro-contaminated basaltic andesitic enclaves within dacite, followed by incomplete mixing to form enclave-bearing layers (bands) of dacite and hybrid andesite; (3) eruption of gabbro-contaminated basaltic andesite as the cinder cone and **bw** lava flow to the west; and (4) eruption of viscous, mingled hybrid lavas of unit **mw**. Tephra from Williams Crater rests on unit **dv** north of Devils Backbone. Compositions of the dacites and their andesitic enclaves (rare in **mw**) indicate that unit **mw** is only slightly younger than **dv** (Bacon, 1990). This, and mild glaciation of **mw** outcrops, point to an age of ca. 35 ka.

Following eruption of these dacites, there is no record preserved of near-summit activity at Mount Mazama. Subsequent volcanism had a different compositional and eruptive character.

PRECLIMACTIC RHYODACITES

The caldera-forming eruption of Mount Mazama was preceded by emplacement of preclimactic rhyodacitic lava domes and flows, at least three of which overlie related, widely dispersed pyroclastic deposits (Bacon, 1983; Bacon and Druitt, 1988). The preclimactic rhyodacites are divided into four map units (**re, rbb, rs, rh**; Figs. 2 and 5F), which are interpreted as magma that leaked from the climactic chamber as it grew. Enclaves in these lavas contain the chemical fingerprints of different andesitic magmas injected into the differentiating chamber (Bacon and Druitt, 1988; Bacon et al., 1994). These andesitic replenishments were parental to the rhyodacites and to complementary phenocryst-rich andesitic scoria and gabbroic crystal mush ejected late in the climactic eruption.

Evolved Pleistocene Rhyodacites Encounter Ice

Evolved Pleistocene rhyodacite (unit **re**; 70%–72% SiO_2) includes the Grouse Hill and Redcloud Cliff flows (Williams, 1942) and a

small dome above Steel Bay (Figs. 4E and 4I), which are the most chemically evolved of the Pleistocene preclimactic rhyodacites (Bacon and Druitt, 1988). A related pumice-fall deposit preserved under the Redcloud Cliff flow has been correlated with the Trego Hot Springs bed of Davis (1985) by Rieck et al. (1992). The aggregate volume of lava is 0.68 km^3, and the estimated magma volume represented by tephra is 1.6 km^3. The porphyritic rhyodacite contains ~15% total phenocrysts of plagioclase, hornblende, orthopyroxene, augite, Fe-Ti oxides, and traces of zircon. Plagioclase and hornblende are as large as 5 mm. Most phenocrysts are similar to crystals in the common microxenoliths (≤6 mm). Partially resorbed rims on plagioclase and tiny Fe-oxide needles in plagioclase cores are characteristic of this unit. Most crystals apparently were derived from Pleistocene intrusive rocks (Bacon and Lowenstern, 2005). Andesitic enclaves (2–25 cm; 59.5%–61% SiO_2) are present but uncommon in the Steel Bay and Grouse Hill domes.

Many exposures of the flanks of the Grouse Hill and Redcloud Cliff flows have 10–15-cm-diameter subhorizontal vitrophyre columns indicative of ice or meltwater chilling (e.g, east end of the Redcloud Cliff flow). The Redcloud Cliff flow has horizontal vitrophyre columns at the base of its northern caldera-facing cliff (Fig. 4I), where the lava must have been bounded by ice. The subaerial(?) Grouse Hill dome rises ~200 m above the pancake-shaped, ice-bounded lava flow, the height of which suggests a minimum ice thickness of >100 m at 2000 m above sea level (asl). Glacial erosion subsequently modified these features and the little **re** dome at Steel Bay. Related paleomagnetic orientations (D.E. Champion, 1983, personal commun.) and the unique petrographic features of the three lava flows indicate that they were erupted in a short time interval, most likely during the Mono Lake paleomagnetic excursion ca. 30 ka. A radiocarbon date on organic carbon beneath the Trego Hot Springs bed at Pyramid Lake in western Nevada is 23,200 ± 300 yr B.P., or a reservoir-corrected calibrated age of ca. 27 ka (Benson et al., 1997; MIS 3.1).

Rhyodacite Dome and Mingled Andesite Tuya at Bear Bluff

The small porphyritic rhyodacite dome at Bear Bluff (**rbb**; 0.015 km^3; 69.5% SiO_2) was extruded, and a contiguous porphyritic andesite tuya (**ab**; 0.12 km^3; 58%–59.5% SiO_2) formed during the LGM ~8 km south of Rim Village (Fig. 5F). Jointing in glassy lava on the southwest slope of the tuya indicates chilling by ice or meltwater. The tuya height suggests an ice thickness of ≥100 m at 1900 m asl. Low hills east and southeast of the tuya are blocks of palagonitic tuff that apparently slid away from the tuya when glacial ice receded, possibly during seismic shaking. The rhyodacite is slightly less differentiated than rhyodacite of the climactic eruption, and the andesite is compositionally similar to enclaves in unit **re** flows. Andesite bombs streaked with rhyodacitic pumice, rare rhyodacite pumice blocks in tuya hyaloclastite, and andesite lava outcrops with layers of coarsely porphyritic, vitric rhyodacitic or hybrid lava ~1–100 cm thick indicate co-eruption of the two magmas, fed from the Mazama climactic magma chamber by commingling dikes or a composite dike that vented at the east-dipping Annie Spring fault (Fig. 2). Unit **rbb** has a $^{40}Ar/^{39}Ar$ isochron age of 24 ± 3 ka (MIS 2.2, LGM).

Sharp Peak Domes

Twelve domes in two en echelon N35°E alignments 4–7 km northeast of the caldera are termed rhyodacite of Sharp Peak (**rs**; 0.05 km^3; 70.5% SiO_2). The porphyritic lava is similar to climactic rhyodacite and was fed by dikes from the climactic chamber (Bacon and Druitt, 1988; Druitt and Bacon, 1989). Sharp Peak has a $^{40}Ar/^{39}Ar$ isochron age of 18 ± 4 ka.

Rare glaciated outcrops near the top of Sharp Peak (1826 m asl) and on another dome indicate later ice was >170 m thick. Glaciation of the domes is consistent with ice-retreat chronology based on sediment cores from Upper Klamath Lake, which indicates significant flux of glacial flour until 16.3 ka, dropping to zero by 14.0 ka (Rosenbaum and Reynolds, 2004). The Upper Klamath Lake record shows that the LGM lasted from 22 to 16 ka and that the percentage of the full-glacial average flour flux was only 10%–30% between 38 and 22 ka, when unit **re** encountered ice. The 22–16 ka range for the LGM suggests that the eruption age of the Bear Bluff units is within the younger part of the $^{40}Ar/^{39}Ar$ error envelope.

Holocene Preclimactic Rhyodacites

The rhyodacitic Llao Rock and Cleetwood flows (Williams, 1942) are shown as Holocene preclimactic rhyodacite lava unit **rh** (1.05 km^3), and related pyroclastic deposits, where sufficiently thick, as unit **rhp** (estimated magma volume 2.5 km^3) in Figures 2, 4D, 4E, 4G, and 5F. Both eruptions began with Plinian columns that left coarse, poorly sorted, lithic-rich deposits near the vent and extensive well-sorted pumice-fall deposits for great distances downwind to the southeast, and ended with extrusion of thick lava flows. Detailed information on Holocene pumice-fall deposits near Crater Lake can be found in Young (1990). The Llao Rock products are the more differentiated, and they preceded the climactic eruption by 200–100 yr. Llao Rock pumice-fall deposits correlate with the Tsoyowata bed of Davis (1978) in Nevada and eastern California (Davis, 1985; Rieck et al., 1992). The Cleetwood flow was still hot when the caldera collapsed, and remobilized lava oozed down the caldera wall and also flowed northeast for at least 1 km beyond its original terminus. Field relations between Cleetwood lava and deposits of the climactic eruption demonstrate the precursory nature of the Cleetwood eruption and the timing of caldera collapse (Bacon, 1983; Kamata et al., 1993).

Products of the Llao Rock and Cleetwood vents can be distinguished chemically and petrographically (Bacon and Druitt, 1988; Druitt and Bacon, 1989). Rhyodacite of the Llao Rock flow, pumice, and dikes ranges from ~70.5–72% SiO_2. Vitrophyre selvages of two dikes in the caldera wall have welded textures and are comparable to the most silicic early erupted pumice (one dike is hidden by a promontory in Fig. 4D); the lava flow typically has ~70.5% SiO_2. Llao Rock rhyodacite contains ~7% phenocrysts of plagioclase (≤1.5 mm, rarely to 3 mm), hornblende (≤1 mm), orthopyroxene (≤1 mm), Fe-Ti oxides (≤0.4 mm), and uncommon augite; hornblende is more abundant (≥orthopyroxene) in the dikes and early erupted pumice. Andesitic enclaves (≤3 cm; rarely to 10 cm; 59.5% SiO_2) are ubiquitous and abundant (~1%) in the lava flow and common in the pumice fall as medium-gray pumiceous clasts or blobs in pumice. Charcoal from beneath the pumice fall yielded a ^{14}C age of 7015 ± 45 yr B.P. (Bacon, 1983) or 7800–7900 cal yr B.P. (Stuiver et al., 1998).

Rhyodacite of the Cleetwood flow and pumice is homogeneous and identical in mineralogy and composition to rhyodacite of the climactic eruption (~70.5% SiO_2). Andesitic enclaves (to ~10 cm; 61.5% SiO_2) are extremely rare. Because the Cleetwood flow was hot and its interior was capable of flow when the caldera collapsed (Bacon, 1983), the Cleetwood eruption occurred <100 yr before the climactic event (Kamata et al., 1993).

THE CLIMACTIC ERUPTION

The climactic eruption of Mount Mazama devastated the terrain for tens of kilometers from the volcano, sent pyroclastic flows over the slopes of Mazama and into every drainage as far as 70 km from their source, and produced ash fall throughout much of the Pacific Northwest. Although there is no written record of the eruption, it nevertheless has been of fundamental

importance to volcanologists in understanding large explosive eruptions, compositional zonation in magma chambers, and collapse calderas (e.g., Williams, 1941, 1942). At least 90% of the ~50 km^3 of magma erupted was compositionally uniform rhyodacitic pumice (70.5% SiO_2; ~10%–15% total phenocrysts of plagioclase, orthopyroxene, augite, hornblende, and Fe-Ti oxides in glass of typically ~72%–72.5% SiO_2; plagioclase + orthopyroxene ± augite ± oxides aggregates common). The remainder was crystal-rich andesitic scoria and mafic crystal mush (47%–61% SiO_2). The petrology and geochemistry of the climactic ejecta are described in Bacon and Druitt (1988), Bacon et al. (1992, 1994), and Druitt and Bacon (1988, 1989), who suggested that rhyodacite magma was generated mainly by crystallization differentiation of basaltic to andesitic sills repeatedly intruded between cumulate mush and overlying derivative silicic magma. Rapid partial crystallization of sills yielded rhyodacitic melt that escaped upward, perhaps by gas-driven filter pressing (Sisson and Bacon, 1999), into the convecting silicic magma.

The climactic eruption took place in two phases (Bacon, 1983; Suzuki-Kamata et al., 1993): (1) a single-vent phase in which a Plinian column from a vent northeast of the summit sent pumice and ash to ~50 km altitude (Young, 1990), resulting in the widespread fall deposit; vent widening and increasing eruption rate eventually caused the column to collapse to lower height, producing pyroclastic flows that deposited the Wineglass Welded Tuff (Williams, 1942; Kamata et al., 1993) in valleys on the north and east flanks of Mazama; and (2) a ring-vent phase, which began at the onset of caldera collapse and produced energetic pyroclastic flows, fed by columns from a number of vents around the foundering cauldron block, which descended radially about Mount Mazama and resulted in a compositionally zoned deposit up to ~100 m thick (Druitt and Bacon, 1986). Throughout these deposits, shown collectively as unit **cd** in Figures 2, 4, and 5F, but especially common in lithic breccia and at the top of ring-vent-phase ignimbrite, are variably fused (0%–50% melt) granodiorite and related lithic blocks (Bacon et al., 1989, 1994; Bacon, 1992) derived from a Pleistocene composite pluton (Bacon and Lowenstern, 2005) that formed the walls of the climactic magma chamber at ~5 km depth (Bacon et al., 1992).

Radiocarbon ages of charcoal associated with deposits of the climactic eruption (Bacon, 1983) have a weighted mean of 6845 ± 50 ^{14}C yr B.P., or a calendar age of ca. 7700 cal yr B.P. (Stuiver et al., 1998). More recent work by Hallet et al. (1997) suggests a somewhat younger age of 6730 ± 40 ^{14}C yr B.P., or 7470–7620 cal yr B.P. Identification of Mazama glass shards in the Greenland Ice Sheet Project 2 (GISP2) core gives 7627 ± 150 cal yr B.P. (Zdanowicz et al., 1999). Although the GISP2 data suggest fine-particle fallout for ~3 yr, the climactic eruption probably lasted only a few days.

Williams (1942) interpreted deposits now mapped as proximal ignimbrite (lithic breccia; Bacon, 1983; Druitt and Bacon, 1986) as probable glacial till. Paleoclimatic reconstructions indicate that the climactic eruption occurred during a relatively warm and dry period (Briles et al., 2005). Any ice would have been restricted to the highest part of Mount Mazama, and valleys on its south flank, especially, would have been ice free at elevations of the caldera rim (~2100 m).

POSTCALDERA VOLCANISM

Volcanic activity in the Crater Lake region since the climactic eruption has been confined to the caldera (Figs. 2 and 5F). Most of the postcaldera products are hidden beneath Crater Lake, where Wizard Island amounts to but 2% of the total of 4 km^3 of postcaldera andesite. Postcaldera eruptive history recently was refined through acoustic mapping of the lake floor (Gardner et al., 2001; Bacon et al., 2002; Nathenson et al., 2006) supplemented by dredged samples and by observation and sampling with a manned submersible (Nelson et al., 1994). Postcaldera andesitic volcanism took place within a few hundred years of caldera collapse, while Crater Lake was filling to nearly its present level. Porphyritic andesites from three vents are recognized: andesite of the central platform (**apc**; 1.06 km^3; 57.5%–62.5% SiO_2), andesite of Merriam Cone (**amc**; 0.34 km^3; 60.5% SiO_2), and andesite of Wizard Island (**aw**; 2.6 km^3; 58.5%–60% SiO_2). Parts of these units vented under water or flowed from then-subaerial vents into the rising lake, leaving a record in foundered shorelines of lava deltas (Bacon et al., 2002). Andesite of the east basin (**ae**; 0.03 km^3; not sampled) is a fourth unit inferred from bathymetry. No tephras from these eruptions have been recognized. The last known postcaldera volcanism produced a hornblende rhyodacite ash bed, recovered in a core taken on the central platform, and a subaqueous dome (**r**; 0.07 km^3; 71.5% SiO_2) on the northeast flank of Wizard Island. Sediment directly beneath the ash in the core has a ^{14}C age of 4240 ± 290 yr B.P. (Nelson et al., 1994) or ca. 4800 cal yr B.P. (Bacon et al., 2002).

NORTHWESTWARD MIGRATION OF THE MAZAMA FOCUS

A shift in the Mazama magmatic focus is evident in the sequential geologic maps of Figure 5. Starting ca. 420 ka, early Mount Mazama vented from what is now the southeast quadrant of the caldera and at Mount Scott (Fig. 5A). Effusive volcanism continued in the same region until ca. 170 ka, constructing the bulk of the edifice (Figs. 5B and 5C). Substantial volumes of dacite effused during this period from flank vents (units **dr**, **dm**, **dg**, and **dcn**). Perhaps because of the load of the Mount Mazama stratovolcano, eruptions subsequent to ca. 170 ka occurred mainly north and northwest of the Mazama summit (Fig. 5D). From 170 to 80 ka, basaltic andesitic to andesitic shields and andesitic domes grew on the northwest, while thick andesitic and dacitic lava flows descended to the north and northeast. The Crater Peak group of vents was active on the south sometime between ca. 130 and 100 ka, apparently involving dacitic magma from Mazama and regional basaltic andesite. Activity 80–40 ka (Fig. 5E) was focused in what is now the west-central part of the caldera but also produced voluminous andesite and dacite from outlying vents (e.g., **arw**, **agc**, and **dc**). The last known products of the Mazama summit region are ca. 35 ka dacitic dome-collapse avalanche deposits (unit **dv**; Fig. 5F). Vents for preclimactic rhyodacite units **re** and **rh** may define the approximate limits of the climactic magma chamber north of the summit, while the rhyodacite domes of Bear Bluff (**rbb**) and the Sharp Peak group (**rs**) apparently were fed by dikes that propagated laterally from the chamber. The climactic eruption started from a vent near the center of the **re**–**rh** cluster and evolved to a ring of vents around the subsiding central block (Bacon, 1983; Suzuki-Kamata et al., 1993). Postcaldera volcanism was concentrated in the western part of the caldera, and the most differentiated magma (**r**) erupted last, in the center of the area of postcaldera andesitic vents. Regional basaltic to andesitic volcanism apparently has persisted in the area since at least ca. 670 ka (a few ages are as old as 1.9 Ma), and the volcanic front appears to have been west of the present High Cascades axis throughout this period.

MAGMA MEETS ICE

Physical features of datable volcanic rocks can indicate ice presence or thickness (Smellie, 2000), and glaciated lava surfaces buried by younger volcanics allow glaciations to be bracketed in time. Diagnostic features range in scale from columnar or polygonal joints and derivative breccias (Lescinsky and Fink, 2000) to the gross morphology of ice-bounded or subglacial lava flows (Lescinsky and Sisson, 1998) and table mountains or tuyas (Mathews, 1947).

Many glaciated surfaces in the caldera walls were noted by Atwood (1935) and Williams (1942). Although alpine glaciers may have been present high on Mount Mazama at virtually any time between ca. 400 ka and caldera collapse, dated times of ice presence tend to coincide with well-established glacial intervals in paleoclimatic chronologies such as marine oxygen isotope stages (MIS; Bowen et al., 1986; Martinson et al., 1987; Bassinot et al., 1994). Table 2 lists examples of the interplay between glacial ice and magma or volcanic rock in the Crater Lake region where the time of ice presence is constrained by K-Ar or $^{40}Ar/^{39}Ar$ geochronology.

Ice-contact structures have not been found in units that erupted during MIS 1, 3 (except unit **re**), 5.1, 5.3, 5.5, 7 (except 7.4), 9, or 11, which presumably would have been ice free, save perhaps at the highest elevations. Correlations with MIS suggest that since eruption of unit **aa**, the last major unit emplaced on the south side of the volcano, ice occupied the major canyons in the south flank of Mazama as many as seven (MIS 8, 7.4, 6, 5.4, 5.2, 4, and 2) or even eight times (MIS 3?). Glacial erosion has modified nearly all Pleistocene regional lavas and their source volcanoes, commonly exposing feeder plugs (e.g., Oasis Butte, Arant Point, Union Peak).

PLEISTOCENE COMPOSITE PLUTON BENEATH MOUNT MAZAMA

Deposits of the climactic eruption contain blocks of granodiorite and minor quartz diorite, aplite, granite, diabase, and granophyre (collectively "granodiorite" hereafter) from a shallow composite pluton beneath Mount Mazama that evidently was the roof and wall rock for the climactic magma chamber (Bacon et al., 1989; Bacon, 1992). Because vents feeding the pyroclastic flows that deposited the blocks were arrayed around an ~5 × 6 km subsiding block (Suzuki-Kamata et al., 1993), the areal extent of the pluton must be at least that great. The granodiorite is similar to erupted dacites in phenocryst, chemical, and radiogenic-isotope compositions (Bacon et al., 1994). Ion microprobe ^{238}U–^{230}Th model ages of zircon from four granodiorite samples indicate that the zircons crystallized at various times between ca. 20 ka and ≥300 ka (Bacon and Lowenstern, 2005). Concentrations of ages near 50–70, ca. 110, and ca. 200 ka correspond to periods of dacitic volcanism. Zircon crystallized at relatively high magma crystallinity during solidification of discrete magma batches because erupted magmas were not zircon saturated. Plutonic rocks that have zircons with a range of ages probably include zircon antecrysts (Charlier et al., 2005) recycled from Quaternary plutonic rocks under conditions that prevented their complete dissolution.

Zircon minimum ages in blocks from around the caldera reflect ages of nearby Mazama vents and may map the distribution of intrusions within the composite pluton. Zircons from two granodiorites collected south and east-southeast of the caldera have model ages >300 ka, ca. 280–150 ka, and ca. 125–80 ka. The intrusive sources of these samples are beneath the quadrant where there are no preserved Mazama lavas younger than ca. 210 ka. The youngest age group probably reflects crystallization of andesitic and dacitic magma such as was erupted elsewhere during ca. 130–100 ka. The older two groups of zircons may have been assimilated from earlier Mazama plutonic rocks ≤400 ka in age, and the oldest from the intrusive remains of the middle-Pleistocene pre-Mazama rhyodacitic magma system. Granodiorite from the west-northwest caldera rim contains zircons with ^{238}U–^{230}Th model ages that cluster strongly ca. 50–70 ka. This sample may represent magma that solidified during the ca. 80–35 ka interval of andesite through dacite volcanism at vents near the west-central part of the caldera. Mafic granodiorite from the east-northeast caldera rim yielded zircons with model ages that suggest

TABLE 2. GLACIAL FEATURES IN THE CRATER LAKE REGION DATED BY K-Ar OR $^{40}Ar/^{39}Ar$

Locality	Units	Feature	Elevation (m)	K-Ar or $^{40}Ar/^{39}Ar$ ages (ka)			MIS	MIS
				Direct ages	Minimum ages	Maximum ages	Bowen*	Bassinot†
Sharp Peak	rs	Glaciated	1650			18 ± 4	2	2.2
Bear Bluff	rbb & ab	Tuya	1900	24 ± 3			2	2.2
Grouse Hill	re	Ice-bounded lava	2000	27§			2	3.1?
Redcloud Cliff	re	Ice contact	2200	27§			2	3.1?
West caldera wall	dwp on aww	Surface	2050		50 ± 3	70 ± 4	4	4.2
Grotto Cove	agc	Ice contact	2010	68 ± 13, 74 ± 10			4	4.2
Steel Bay	aww on dsb	Surface	2070		70 ± 4	116 ± 5, 116 ± 9	4, 5b, 5d	4.2, 5.2, 5.4
W Cleetwood Cove	abl on till	Till	1900		102 ± 10		5d	5.4
Pumice Point	alu	Ice contact	1900	117 ± 3			5d	5.4
Pumice Point	alu on all	Surface	1900		117 ± 3	122 ± 20	5d, 6	5.4, 6.2
Roundtop	ar	Ice-bounded lava	1950	159 ± 13			6	6.4, 6.6
N of Castle Creek	dcn on aa	Surface	1770		216 ± 4	258 ± 7	7, 8	7.4, 8.2, 8.4
S of Garfield Peak	ag on aa	Surface	2100		224 ± 9	269 ± 12	7, 8	7.4, 8.2, 8.4
Dutton Cliff & N of Kerr Notch	aa	Ice contact	2390 & 2090	231 ± 10, 244 ± 4, 245 ± 10			7 8 8	7.4 8.2 8.2
Munson Ridge	dm	Ice contact	2040	276 ± 11			8	8.4
Arant Point	at	Tuya	2000	297 ± 12			8	8.6
Sentinel Rock & Grotto Cove	dr on ak	Surface	2000 & 1890		306 ± 5, 336 ± 6	340 ± 6, 341 ± 8	10	10.2, 10.4
Southwest shore	arv on db	Surface	1890		302 ± 10	351 ± 12	10	10.2, 10.4
Sun Notch	ak on db	Sediment	2100		340 ± 6, 341 ± 8	354 ± 4, 382 ± 8	10	10.2, 10.4, 11.22

*MIS Bowen is marine oxygen isotope stage terminology of Bowen et al. (1986).
†MIS Bassinot is marine oxygen isotope stage terminology of Bassinot et al. (1994).
§Calibrated radiocarbon age of soil below correlative tephra (Benson et al., 1997).

crystallization during the ca. 130–100 ka and ca. 80–35 ka periods, along with many zircons that possibly crystallized in nonerupted magma from the ca. 27 ka evolved Pleistocene rhyodacite episode. The zircon data thus suggest that the youngest intrusion(s) are north of an east-west midline across the caldera.

TIME–VOLUME–COMPOSITION RELATIONS

A major goal of the present study is to document ages, volumes, and compositions of eruptive units for Mount Mazama and volcanoes of the surrounding region. Burial of older units by younger ones and repeated glacial erosion complicate estimation of volumes and produce ever-larger uncertainty for units of increasing age (see Singer et al., 1997, for a thoughtful discussion). Pyroclastic and laharic material deposited on ice or in valleys, and thin intracanyon lava flows, would have been removed by glacial advances. Absolute durations of volcanic episodes are poorly known because of analytical uncertainties in bracketing ages. Consequently, the record is incomplete and fragmentary, and the interpretations presented here are subjective.

In simplest terms, Mazama vented <1% basaltic andesite, 42% andesite, 15% dacite, and 43% rhyodacite in its lifetime. Prior to 30 ka, there was no rhyodacite, and the proportion of andesite to dacite was 2:1. In the same period, regional lavas were <1% basalt, 58% basaltic andesite, and 42% andesite, and the Timber Crater shield accounted for nearly all of the andesite. The distribution of average or bulk compositions of units through time is not uniform (Fig. 6). After an ~70 k.y. initial dacite-dominated period, Mazama produced mainly andesite until again venting a substantial volume of dacite at 70 ka. Bona fide rhyodacite did not appear until ca. 27 ka and thereafter was dominant until postcaldera time, when andesite accounted for 98% of the erupted volume.

Although units are named for representative compositions (Figs. 2 and 6), the range within many units is substantial (Fig. 7A). Following eruption of pre-Mazama rhyodacites, maximum SiO_2 from 420 to 110 ka was 67%. Subsequently, SiO_2 climbed to 68% at ca. 70 ka and >70% after 30 ka. From 400 to almost 30 ka, at least some andesite lava was erupted in virtually every episode, and many produced mafic andesite lava or enclaves that extended the silica range at Mazama down into that of regional lavas. Excepting enclaves in mingled lava at Williams Crater and cumulate blocks in the climactic ejecta, the most mafic samples are regional lavas. These observations are the basis for the model in which the Mazama focus was fed by parental magmas similar to those erupted from regional monogenetic and shield volcanoes, and the lavas that were erupted at Mazama were a consequence of the degree that crystallization differentiation, magma mixing, and recycling of cumulates and plutonic material operated during a given magmatic episode.

Cumulative Volume, Eruption Rates, and Magma Production

The episodic nature of volcanism in the Crater Lake region is evident on a plot of cumulative volume versus time (Fig. 7B). Because the absolute durations of eruption of individual units are not well known, volumes are plotted at times representative of each unit. Dashed lines represent alternative interpretations of constant (minimum) eruption rates for the more voluminous and long-lasting units (e.g., **ak**, **aa**). The long-term eruption rate for all of Mazama prior to 27 ka based on Figure 7B is ~0.15 km^3 $k.y.^{-1}$ (but see following), which is identical to that given by Harford et al. (2002) for 170 k.y. of activity at the andesitic South Soufrière Hills–Soufrière Hills center on Montserrat. In the last 80 k.y., where the record is more detailed, there was a 10–15 k.y. interval in which the mean eruption rate was ~0.8 km^3 $k.y.^{-1}$, followed by ~40 k.y. in which the mean rate was only ~0.09 km^3 $k.y.^{-1}$. Both intervals produced thin cone-building lavas, large single flows, and dacitic pyroclastics. As pointed out by Hildreth and Lanphere (1994), stratovolcanoes commonly grow in spurts superimposed on relatively steady long-term productivity, and Mazama is no exception. The 0.8 km^3 $k.y.^{-1}$ Mazama rate is similar to long-term rates for some andesitic arc volcanoes, e.g., 0.6 km^3 $k.y.^{-1}$ for El Misti (Thouret et al., 2001), and ~0.9 km^3 $k.y.^{-1}$ for Ruapehu (Gamble et al., 2003), and 0.9 km^3 $k.y.^{-1}$ for the past 2.5 k.y. at Ngauruhoe (Hobden et al., 2002). The highest quantifiable short-term Mazama rate is the ~8 km^3 $k.y.^{-1}$ minimum for the inferred <500 yr of postcaldera andesite effusion (Bacon et al., 2002), which is comparable to major cone-building episodes at Mount Adams and other arc volcanoes cited by Hildreth and Lanphere (1994).

The total volume of Mazama eruptive units that comprise the edifice, obtained by summing volume estimates of individual units older than 30 ka in age, is 58 km^3 (Fig. 7B). The factor of two discrepancy between this and the 112 km^3 GIS estimate for reconstructed Mount Mazama is due to the methods employed to approximate individual map unit volumes and to incomplete knowledge of the geology of the foundered summit and beneath Crater Lake. The GIS-based estimate is likely to be the more accurate for the complete edifice volume, which itself must underestimate total erupted volume; it yields a long-term average eruption rate of 0.29 km^3 $k.y.^{-1}$ for 420–30 ka. In comparison with other Cascade volcanoes with published, well-constrained eruptive histories, the Mazama rate is indistinguishable from the ~0.3 km^3 $k.y.^{-1}$ rates of Black Buttes/Mount Baker (Hildreth et al., 2003a) but is somewhat less than 0.4–0.7 km^3 $k.y.^{-1}$ at Mount Adams (Hildreth and Lanphere, 1994). Addition of a magmatic volume estimate of 64 km^3 for all products younger than 30 ka in age, mainly climactic ejecta, yields a total eruptive output of 176 km^3 in the past ~420 k.y., or a long-term rate of 0.42 km^3 $k.y.^{-1}$.

Estimating magma *production* rates is a far less satisfactory endeavor than constraining eruption rates. Because magmas that erupted from Mount Mazama show the effects of crystallization differentiation, with or without assimilation, there must be a very large volume of accumulated crystals in the crust below. A fraction of these crystals has been recycled into most Mazama lavas, in regional lavas vented close by, and in the climactic ejecta. It also is clear that substantial amounts of differentiated magma froze in the upper crust to form a composite pluton (Bacon and Lowenstern, 2005). We speculate that the amount of nonerupted magma is several times the total volume erupted. The rhyodacitic magma ejected in the climactic eruption was generated at an average rate of ~2.5 km^3 $k.y.^{-1}$ over 20 k.y., but the crystallization differentiation mechanism implies that the total magma production rate for that period must have been several times as large.

The eruption rate since 300 ka for shield and monogenetic volcanoes in the Crater Lake region is ~0.07 km^3 $k.y.^{-1}$, but is only ~0.02 km^3 $k.y.^{-1}$ if the Union Peak and Timber Crater shields are excluded. Normalized to arc length, these values are ~2 and ~0.6 km^3 $m.y.^{-1}$ km^{-1}, respectively. For comparison, Sherrod and Smith (1990) gave 4 km^3 $m.y.^{-1}$ km^{-1} over the past 0.73 m.y. for the mafic-shield–dominated 110 km of arc from 44°N to 43°N, between Mount Mazama and Three Sisters volcanoes, and Hasenaka (1994) indicated ~4 km^3 $m.y.^{-1}$ km^{-1} for the last 1 m.y. for shields and monogenetic volcanoes of the Michoacán–Guanajuato volcanic field, Mexico.

Regional and Local Magmatic Pulses

As at Mounts Adams and Baker (Hildreth and Lanphere, 1994; Hildreth et al., 2003a), major additions to the Mazama edifice occurred in a few pulses (Fig. 7B). These may have been similar to the onset of the ca. 80–30 ka record in which a high eruption rate lasting 10–15 k.y.

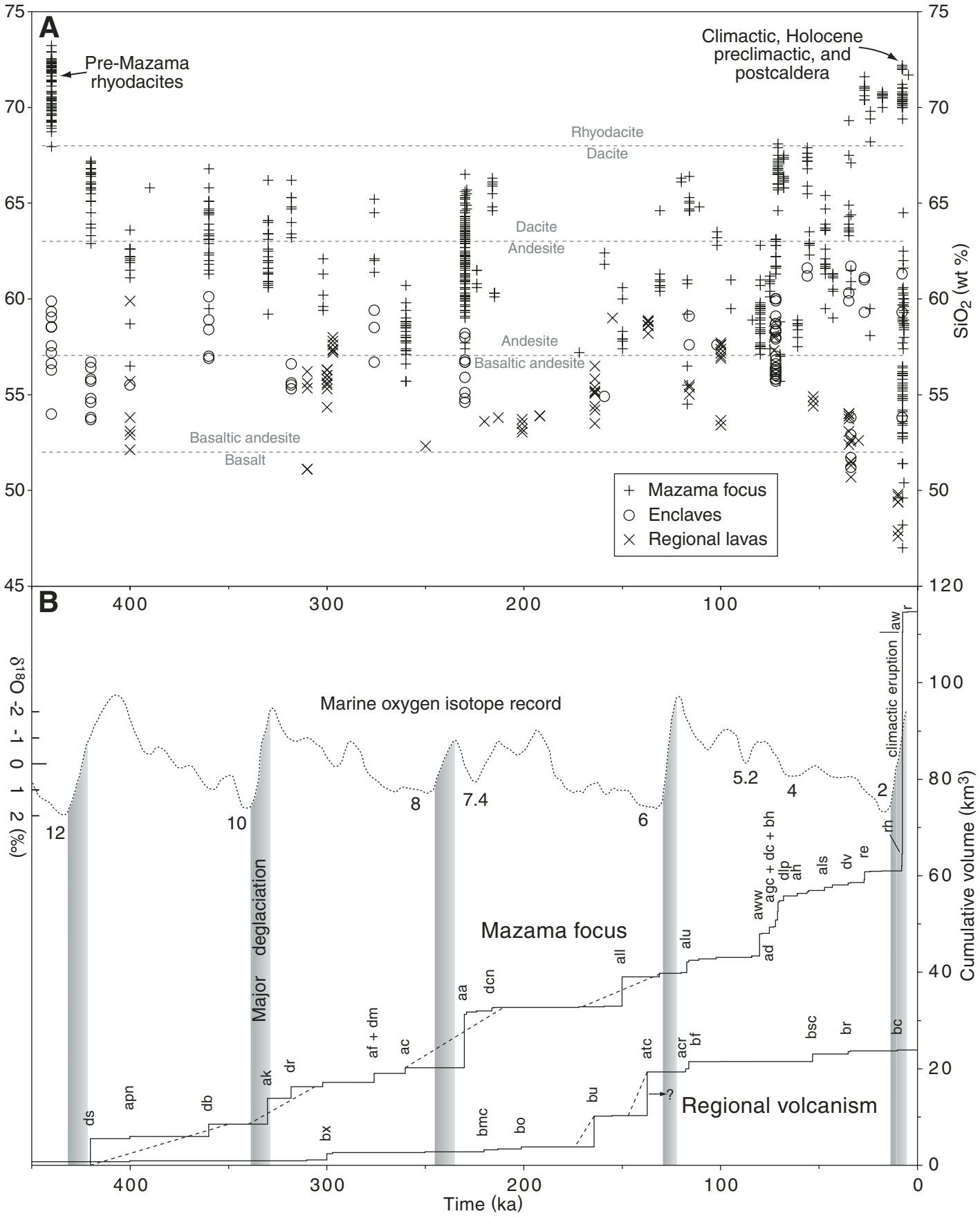

Figure 7. Silica and volume versus time. Data for some units are plotted at representative or assumed times (e.g., regional lavas at 400 ka). (A) Whole-rock SiO_2 content (same data set as for Figure 1). All samples from individual units are plotted at single times even though eruptive durations for some units may have been substantial. Pre-Mazama rhyodacites (units rsc, rcs, rpb) and their enclaves are plotted for reference at 440 ka. Holocene Mazama-focus samples with ≤55% SiO_2 are crystal cumulates; most climactic samples with ≤61% SiO_2 probably have lost some melt. Enclaves typically are frozen undercooled phenocryst-poor magma; however, of those plotted at 72 ka, all but the most silicic have lost residual melt by gas-driven filter pressing. (B) Cumulative magma volume erupted versus time for Mount Mazama and for regional shield and monogenetic volcanoes. Volumes are estimates for reconstructed mapped units (Table A3; see text footnote 1); total Mazama edifice volume was greater (see text). Volumes of individual units are plotted at representative times. Possible durations of some major eruptive episodes are indicated by dashed segments of cumulative volume plot. Marine oxygen isotope (MIS) record (Bassinot et al., 1994, their Fig. 7), with selected numbered MIS, is shown for reference. Major continental deglaciations are indicated by shaded vertical bars.

was followed by a background rate an order of magnitude lower. Major pulses in regional volcanism reflect growth of Union Peak and Timber Crater shield volcanoes, at what amounts to point sources, above a low background of monogenetic volcanism.

The pulses in eruption rate could be caused by variations in magma supply from the mantle or by changes in the upper crustal environment induced by tectonic stress or glacial loading. Isotopic and trace-element compositional variation among major eruptive units (Bacon et al., 1994) indicates that each had its own, commonly unique, mantle-derived parent magma(s). Exactly when a mantle domain happened to supply Mazama seems unlikely to be related to upper crustal external controls, whereas millennial-scale eruption rate may have been affected by such a factors.

At least some of the pulses in the Mazama plot may be related in a loose way to rapid deglaciation following MIS 12, 10, 8, 6, 5.2, and 2 (Fig. 7B). This observation is conceptually similar to that of Singer et al. (1997), who noted that lacunae (hiatuses in the volcanic record) corresponding to glacial maxima were each followed by renewed volcanism at the Tatara–San Pedro complex (36°S), Chile. The Timber Crater volcano possibly generated a large volume of andesite because ice loading during the long penultimate glaciation (MIS 6) promoted storage and differentiation, and this magma vented when the ice rapidly melted. In the case of the climactic magma chamber, only the lateral-dike-fed vents at Bear Bluff and the Sharp Peak domes were active around the time of the LGM (MIS 2) when thick ice must have been present on Mazama and its flanks (assuming the ca. 27 ka age of unit **re** is correct). Although there are many examples globally of voluminous silicic eruptions in areas free of glacial influence and the more-voluminous Holocene rhyodacitic eruptions at Mazama followed ice retreat by several thousand years, suppression of volcanism by ice loading may have contributed to accumulation of the large volume of vapor-saturated rhyodacitic magma that ultimately vented in the climactic eruption.

Silicic Magma Generation

The Mazama time–volume–composition relations (Figs. 6 and 7) provide a framework for determining what conditions favored silicic magma production. Repeated eruption of mafic andesite (e.g., ca. 210–125 ka, Fig. 7A) would suggest rapid throughput of small magma batches that could leave behind cumulates but would not be likely to lodge in the upper crust and differentiate further. Voluminous dacitic eruptions at Mazama may have required preheating of the upper crust sufficient to keep any stalled andesitic magma from freezing completely, allowing time for accumulation of dacitic residual melt. The initial ca. 420–350 ka dacite-dominated interval followed voluminous pre-Mazama rhyodacite effusion, suggesting a warm upper crust conducive to prolonged differentiation. By ca. 170 ka, Mazama was erupting mafic andesite and building the shield below present-day Llao Rock, northwest of the former central vent. The Union Peak and Timber Crater shields were roughly contemporary with this Mazama volcanism. Perhaps the ability of Mazama to subsequently produce dacitic magma was related to a sustained increase in regional magma flux from the mantle that, after a few tens of thousands of years, led to a succession of relatively long-lived upper crustal magma reservoirs that produced eruptible volumes of dacitic magma from ca. 120 ka until ca. 35 ka.

Between ca. 55 and ca. 35 ka, another pulse in regional volcanism released basaltic andesite at Scoria Cone, magnesian basaltic andesite at Red Cone, and, possibly also during this interval, high-alumina olivine tholeiite at a vent 3.5 km east-northeast of Oasis Butte (north of Fig. 2). Shortly after eruption of primitive magma from Red Cone, the first rhyodacite appeared (**re**). It may not be coincidental that growth of the shallow climactic magma chamber closely followed this regional pulse of primitive magmatism (Figs. 6 and 7A). Postglacial venting of primitive high-alumina olivine tholeiite at Castle Point suggests that the regional mantle magma flux remained high, feeding the roots of the Mazama system and helping to sustain a growing volume of convecting rhyodacitic magma at just a few kilometers depth. In contrast, the little postcaldera rhyodacite dome (0.074 km^3) probably consists of melt segregated from the freezing remains of the andesitic postcaldera Mazama system.

CONCLUSIONS

The andesite-dominated Mount Mazama edifice was built on an earlier silicic lava field, a site of long-term magmatic focusing probably controlled by regional tectonics. Mazama eruptive history began with a mainly dacitic interval that may reflect a relatively warm upper crustal thermal regime following pre-Mazama rhyodacite magmatism. Subsequently, an andesite-dominated period built much of the edifice height and volume, episodically produced dacite, and ended in dacite effusion ca. 215 ka. After ~45 k.y. of minor activity or inactivity, renewed volcanism starting ca. 170 ka built a large andesitic shield northwest of the Mazama summit while the two largest regional shield volcanoes also were active. This led into a post-120 ka period of mainly andesitic and dacitic flank lava effusion, punctuated at ca. 70 ka by voluminous dacitic lava flows and pumice falls from widely distributed vents. The late history of Mazama, ca. 55–35 ka, produced central-vent andesite lavas, flank dacite, and summit dacite domes. Regional volcanism was vigorous during this period. Coincidence of rhyodacitic eruptions, beginning ca. 27 ka, between late Pleistocene and postglacial venting of unusually primitive basaltic andesite and tholeiitic basalt in the surrounding region suggests that increased thermal and mass input beneath Mazama contributed to establishment and sustenance of the climactic magma chamber. The eruptive history of Mount Mazama spanning 420 k.y. suggests that a long period of thermal conditioning of the middle to upper crust was necessary before a shallow silicic magma body could accumulate and grow large enough to produce a caldera-forming eruption.

The ~0.4 km^3 $k.y.^{-1}$ long-term average eruption rate at Mount Mazama (~0.3 km^3 $k.y.^{-1}$ for 420–30 ka) is substantial but not exceptional in comparison to those of other arc volcanoes. Apart from two shield volcanoes, the 0.02 km^3 $k.y.^{-1}$ regional eruption rate of nearby monogenetic volcanoes since 300 ka (~0.6 km^3 $m.y.^{-1}$ km^{-1} along the arc) is unimpressive. However, ubiquitous fragments of crystal mush and plutonic rock in Mazama lavas, ejection of cumulate mush and plutonic rocks in the climactic eruption, and the dominance of crystallization differentiation as the principal mechanism of magma evolution are compelling evidence for the presence of a large volume of intrusive and cumulate material that may amount to several times that of the magma erupted. A combination of a long volcanic history, silicic magma recently erupted from distributed vents without spatially intervening mafic to intermediate volcanism, and unusually vigorous or primitive regional volcanism would identify a volcanic center as prone to catastrophic eruption from a shallow magma body.

ACKNOWLEDGMENTS

Argon extractions and mass spectrometry were ably performed by James Saburomaru and Jerry Von Essen. In a companion study, Duane Champion collected and measured innumerable rock cores to determine paleomagnetic poles that enabled correlations and constrained ages for many units. Andrei Sarna-Wojcicki shared his encyclopedic knowledge of western U.S. tephrochronology, and John Barron advised us on paleoclimate considerations. Geologic mapping by Bacon was aided by William Bartling, Tracey Felger, Shir Filler, Anne Gartner, Maura Hanning, Marc Hirschmann, Jacob Madden, Steven McKnight, Carl Michelsen, Marcus Moench, Steven Novak, Maribeth Price, Patricia Weston, and Simon Young. Dave Ramsey and Dillon Dutton facilitated geographic information systems (GIS) map compilation and production of the caldera wall panoramas, and Ramsey calculated the volume of reconstructed Mount Mazama. We thank Crater Lake National Park for permission to collect samples and for logistical support for work within the caldera. Wes Hildreth and Duane Champion provided helpful comments on the draft manuscript, and *GSA Bulletin* reviews by Anita Grunder and Dennis Geist led to clearer and more concise presentation. We are especially indebted to Wes Hildreth whose eruptive history papers showed us the way along the long road to completing the present manuscript.

REFERENCES CITED

Atwood, W.W., Jr., 1935, The glacial history of an extinct volcano, Crater Lake National Park: The Journal of Geology, v. 43, p. 142–168.

Bacon, C.R., 1983, Eruptive history of Mount Mazama and Crater Lake caldera, Cascade Range, U.S.A.: Journal of Volcanology and Geothermal Research, v. 18, p. 57–115, doi: 10.1016/0377-0273(83)90004-5.

Bacon, C.R., 1986, Magmatic inclusions in silicic and intermediate volcanic rocks: Journal of Geophysical Research, v. 91, p. 6091–6112.

Bacon, C.R., 1989, Crystallization of accessory phases in magmas by local saturation adjacent to phenocrysts: Geochimica et Cosmochimica Acta, v. 53, p. 1055–1066, doi: 10.1016/0016-7037(89)90210-X.

Bacon, C.R., 1990, Calc-alkaline, shoshonitic, and primitive tholeiitic lavas from monogenetic volcanoes near Crater Lake, Oregon: Journal of Petrology, v. 31, p. 135–166.

Bacon, C.R., 1992, Partially melted granodiorite and related rocks ejected from Crater Lake caldera, Oregon: Transactions of the Royal Society of Edinburgh, Earth Sciences, v. 83, p. 27–47.

Bacon, C.R., 2007, Geologic map of Mount Mazama and Crater Lake caldera, Oregon: U.S. Geological Survey Scientific Investigations Map SIM 2832, scale 1:24,000 and 1:50,000 (in press).

Bacon, C.R., and Druitt, T.H., 1988, Compositional evolution of the zoned calcalkaline magma chamber of Mount Mazama, Crater Lake, Oregon: Contributions to Mineralogy and Petrology, v. 98, p. 224–256, doi: 10.1007/BF00402114.

Bacon, C.R., and Lanphere, M.A., 1990, The geologic setting of Crater Lake, Oregon, *in* Drake, E.T., Larson, G.L., Dymond, J., and Collier, R., eds., Crater Lake: An Ecosystems Study: San Francisco, American Association for the Advancement of Science, Pacific Division, p. 19–27.

Bacon, C.R., and Lowenstern, J.B., 2005, Late Pleistocene granodiorite source for recycled zircon and phenocrysts in rhyodacite lava at Crater Lake, Oregon: Earth and Planetary Science Letters, v. 233, p. 277–293, doi: 10.1016/j.epsl.2005.02.012.

Bacon, C.R., and Nathenson, M., 1996, Geothermal resources in the Crater Lake area, Oregon: U.S. Geological Survey Open-File Report 96-663, 34 p.

Bacon, C.R., Adami, L.H., and Lanphere, M.A., 1989, Direct evidence for the origin of low-^{18}O silicic magmas—Quenched samples of a magma chamber's partially-fused granitoid walls: Earth and Planetary Science Letters, v. 96, p. 199–208, doi: 10.1016/0012-821X(89)90132-5.

Bacon, C.R., Newman, S., and Stolper, E., 1992, Water, CO_2, Cl, and F in melt inclusions in phenocrysts from three Holocene explosive eruptions, Crater Lake, Oregon: The American Mineralogist, v. 77, p. 1021–1030.

Bacon, C.R., Gunn, S.H., Lanphere, M.A., and Wooden, J.L., 1994, Multiple isotopic components in Quaternary volcanic rocks of the Cascade arc near Crater Lake, Oregon: Journal of Petrology, v. 35, p. 1521–1556.

Bacon, C.R., Bruggman, P.E., Christiansen, R.L., Clynne, M.A., Donnelly-Nolan, J.M., and Hildreth, W., 1997a, Primitive magmas at five Cascade volcanic fields—Melts from hot, heterogeneous sub-arc mantle, *in* Nixon, G.T., Johnston, A.D, and Martin, R.F., eds., Nature and Origin of Primitive Magmas at Subduction Zones: Canadian Mineralogist, v. 35, p. 397–423.

Bacon, C.R., Mastin, L.G., Scott, K.M., and Nathenson, M., 1997b, Volcano and earthquake hazards in the Crater Lake region, Oregon: U.S. Geological Survey Open-File Report 97-487, 32 p.

Bacon, C.R., Lanphere, M.A., and Champion, D.E., 1999, Late Quaternary slip rate and seismic hazards of the West Klamath Lake fault zone near Crater Lake, Oregon Cascades: Geology, v. 27, p. 43–46, doi: 10.1130/0091-7613(1999)027<0043:LQSRAS>2.3.CO;2.

Bacon, C.R., Gardner, J.V., Mayer, L.A., Buktenica, M.W., Dartnell, P., Ramsey, D.W., and Robinson, J.E., 2002, Morphology, volcanism, and mass wasting in Crater Lake, Oregon: Geological Society of America Bulletin, v. 114, p. 675–692, doi: 10.1130/0016-7606(2002)114<0675:MVAMWI>2.0.CO;2.

Bassinot, F.C., Labeyrie, L.D., Vincent, E., Quidelleur, X., Shackleton, N.J., and Lancelot, Y., 1994, The astronomical theory of climate and the age of the Brunhes-Matuyama magnetic reversal: Earth and Planetary Science Letters, v. 126, p. 91–108, doi: 10.1016/0012-821X(94)90244-5.

Benson, L.V., Smoot, J.P., Kashgarian, M., Sarna-Wojcicki, A.M., and Burdett, J.W., 1997, Radiocarbon ages and environments of deposition of the Wono and Trego Hot Springs tephra layers in the Pyramid Lake subbasin, Nevada: Quaternary Research, v. 47, p. 251–260, doi: 10.1006/qres.1997.1897.

Bleil, U., and Gard, G., 1989, Chronology and correlation of Quaternary magnetostratigraphy and nannofossil biostratigraphy in Norwegian-Greenland Sea sediments: Geologische Rundschau, v. 78, p. 1173–1187, doi: 10.1007/BF01829339.

Bowen, D.Q., Richmond, G.M., Fullerton, D.S., Sibrava, V., Fulton, R.J., and Velichko, A.A., 1986, Correlation of Quaternary glaciations in the Northern Hemisphere, *in* Sibrava, V., Bowen, D.Q., and Richmond, G.M., eds., Quaternary Glaciations in the Northern Hemisphere: Quaternary Science Reviews, v. 5, p. 509–510 and chart 1.

Briles, C.E., Whitlock, C., and Bartlein, P.J., 2005, Postglacial vegetation, fire, and climate history of the Siskiyou Mountains, Oregon, USA: Quaternary Research, v. 64, p. 44–56, doi: 10.1016/j.yqres.2005.03.001.

Bruggman, P.E., Bacon, C.R., Aruscavage, P.J., Lerner, R.W., Schwarz, L.J., and Stewart, K.C., 1987, Chemical analyses of rocks and glass separates from Crater Lake National Park and vicinity, Oregon: U.S. Geological Survey Open-File Report, 87-57, 36 p.

Bruggman, P.E., Bacon, C.R., Mee, J.S., Pribble, S.T., and Siems, D.F., 1989, Chemical analyses of volcanic rocks from monogenetic and shield volcanoes near Crater Lake, Oregon: U.S. Geological Survey Open-File Report 89-562, 15 p.

Bruggman, P.E., Bacon, C.R., Mee, J.S., Pribble, S.T., and Siems, D.F., 1993, Chemical analyses of pre-Mazama silicic volcanic rocks, inclusions, and glass separates, Crater Lake, Oregon: U.S. Geological Survey Open-File Report 93-314, 20 p.

Charlier, B.L.A., Wilson, C.J.N., Lowenstern, J.B., Blake, S., van Calsteren, P.W., and Davidson, J.P., 2005, Magma generation at a large, hyperactive silicic volcano (Taupo, New Zealand) revealed by U-Th and U-Pb systematics in zircons: Journal of Petrology, v. 46, p. 3–32, doi: 10.1093/petrology/egh060.

Dalrymple, G.B., 1989, The GLM continuous laser system for $^{40}Ar/^{39}Ar$ dating: Description and performance characteristics: U.S. Geological Survey Bulletin 1890, p. 89–96.

Davis, J.O., 1978, Quaternary tephrachronology of the Lake Lahontan area, Nevada and California: Nevada Archeological Survey Research Paper 7, 134 p.

Davis, J.O., 1985, Correlation of late Quaternary tephra layers in a long pluvial sequence near Summer Lake, Oregon: Quaternary Research, v. 23, p. 38–53, doi: 10.1016/0033-5894(85)90070-5.

Diller, J.S., and Patton, H.B., 1902, The geology and petrography of Crater Lake National Park: U.S. Geological Survey Professional Paper 3, 167 p.

Druitt, T.H., and Bacon, C.R., 1986, Lithic breccia and ignimbrite erupted during the collapse of Crater Lake caldera, Oregon: Journal of Volcanology and Geothermal Research, v. 29, p. 1–32, doi: 10.1016/0377-0273(86)90038-7.

Druitt, T.H., and Bacon, C.R., 1988, Compositional zonation and cumulus processes in the Mount Mazama magma chamber, Crater Lake, Oregon: Transactions of the Royal Society of Edinburgh, Earth Sciences, v. 79, p. 289–297.

Druitt, T.H., and Bacon, C.R., 1989, Petrology of the zoned calcalkaline magma chamber of Mount Mazama, Crater Lake, Oregon: Contributions to Mineralogy and Petrology, v. 101, p. 245–259, doi: 10.1007/BF00375310.

Druitt, T.H., Edwards, L., Mellors, R.M., Pyle, D.M., Sparks, R.S.J., Lanphere, M., Davies, M., and Barriero, B., 1999, Santorini Volcano: Geological Society [London] Memoir 19, 165 p.

Dungan, M.A., Wulff, A., and Thompson, R., 2001, Eruptive stratigraphy of the Tatara–San Pedro complex, 36°S, Southern volcanic zone, Chilean Andes: Reconstruction method and implications for magma evolution at long-lived arc volcanic centers: Journal of Petrology, v. 42, p. 555–626, doi: 10.1093/petrology/42.3.555.

Fiebelkorn, R.B., Walker, G.W., MacLeod, N.S., McKee, E.H., and Smith, J.G., 1982, Index to K-Ar age determinations for the state of Oregon: U.S. Geological Open-File Report 82-596, 40 p.

Fitzgibbon, T.T., and Wentworth, C.M., 1991, ALACARTE user interface-AML code and demonstration maps: U.S. Geological Survey Open-File Report 91-587A, version 1.0.

Frey, H.M., Lange, R.A., Hall, C.M., and Delgado-Granados, H., 2004, Magma eruption rates constrained by $^{40}Ar/^{39}Ar$ chronology and GIS for the Ceboruco–San Pedro volcanic field, Mexico: Geological Society of America Bulletin, v. 116, p. 259–276, doi: 10.1130/B25321.1.

Gamble, J.A., Price, R.C., Smith, I.E.M., McIntosh, W.C., and Dunbar, N.W., 2003, $^{40}Ar/^{39}Ar$ geochronology of magmatic activity, magma flux and hazards at Ruapehu volcano, Taupo volcanic zone, New Zealand: Journal of Volcanology and Geothermal Research, v. 120, p. 271–287, doi: 10.1016/S0377-0273(02)00407-9.

Gardner, J.V., Dartnell, P., Hellequin, L., Bacon, C.R., Mayer, L.A., Buktenica, M.W., and Stone, J.C., 2001, Bathymetry and selected perspective views of Crater Lake, Oregon: U.S. Geological Survey, Water Resources Investigations Report 01-4046, 2 sheets.

Gill, J.B., 1981, Orogenic Andesites and Plate Tectonics: Berlin, Springer-Verlag, 390 p.

Hallet, D.J., Hills, L.V., and Clague, J.J., 1997, New accelerator mass spectrometry radiocarbon ages for the Mazama tephra layer from Kootenay National Park, British Columbia, Canada: Canadian Journal of Earth Sciences, v. 34, p. 1202–1209.

Harford, C.L., Pringle, M.S., Sparks, R.S.J., and Young, S.R., 2002, The volcanic evolution of Montserrat using $^{40}Ar/^{39}Ar$ geochronology, *in* Druitt, T.H., and Kokelaar, B.P., eds., The Eruption of Soufrière Hills Volcano, Montserrat, from 1995 to 1999: Geological Society [London] Memoir 21, p. 93–113.

Hart, W.K., Aronson, J.L., and Mertzman, S.A., 1984, Areal distribution and age of low-K, high-alumina olivine tholeiite magmatism in the northwestern Great Basin: Geological Society of America Bulletin, v. 95, p. 186–195, doi: 10.1130/0016-7606(1984)95<186:ADAAOL>2.0.CO;2.

Hasenaka, T., 1994, Size, distribution, and magma output rate for shield volcanoes of the Michoacán–Guanajuato volcanic field, central Mexico: Journal of Volcanology and Geothermal Research, v. 63, p. 13–31, doi: 10.1016/0377-0273(94)90016-7.

Hildreth, W., and Lanphere, M.A., 1994, Potassium-argon geochronology of a basalt-andesite-dacite arc system—The Mount Adams volcanic field, Cascade Range of southern Washington: Geological Society of America Bulletin, v. 106, p. 1413–1429, doi: 10.1130/0016-7606(1994)106<1413:PAGOAB>2.3.CO;2.

Hildreth, W., Fierstein, J., and Lanphere, M., 2003a, Eruptive history and geochronology of the Mount Baker volcanic field, Washington: Geological Society of America Bulletin, v. 115, p. 729–764, doi: 10.1130/0016-7606(2003)115<0729:EHAGOT>2.0.CO;2.

Hildreth, W., Lanphere, M.A., and Fierstein, J., 2003b, Geochronology and eruptive history of the Katmai volcanic cluster, Alaska Peninsula: Earth and Planetary Science Letters, v. 214, p. 93–114, doi: 10.1016/S0012-821X(03)00321-2.

Hildreth, W., Lanphere, M.A., Champion, D.E., and Fierstein, J., 2004, Rhyodacites of the Kulshan caldera, north Cascades of Washington: Postcaldera lavas that span the Jaramillo: Journal of Volcanology and Geothermal Research, v. 130, p. 227–264, doi: 10.1016/S0377-0273(03)00290-7.

Hobden, B.J., Houghton, B.F., and Nairn, I.A., 2002, Growth of a young, frequently active composite cone: Ngauruhoe volcano, New Zealand: Bulletin of Volcanology, v. 64, p. 392–409, doi: 10.1007/s00445-002-0216-3.

Jicha, B.R., and Singer, B.S., 2006, Volcanic history and magmatic evolution of Seguam Island, Aleutian Island arc, Alaska: Geological Society of America Bulletin, v. 118, no. 7–8, p. 805–822, doi: 10.1130/B25861.1

Kamata, H., Suzuki-Kamata, K., and Bacon, C.R., 1993, Deformation of the Wineglass Welded Tuff and the timing of caldera collapse at Crater Lake, Oregon: Journal of Volcanology and Geothermal Research, v. 56, p. 253–265, doi: 10.1016/0377-0273(93)90019-N.

Lanphere, M.A., 2000, Comparison of conventional K-Ar and $^{40}Ar/^{39}Ar$ dating of young mafic volcanic rocks: Quaternary Research, v. 53, p. 294–301, doi: 10.1006/qres.1999.2122.

Leaver, D.S., Mooney, W.D., and Kohler, W.M., 1984, A seismic refraction study of the Oregon Cascades: Journal of Geophysical Research, v. 89, p. 3121–3134.

Lescinsky, D.T., and Fink, J.H., 2000, Lava and ice interaction at stratovolcanoes—Use of characteristic features to determine past glacial extents and future volcanic hazards: Journal of Geophysical Research, v. 105, p. 23,711–23,726.

Lescinsky, D.T., and Sisson, T.W., 1998, Ridge-forming, ice-bounded lava flows at Mount Rainier, Washington: Geology, v. 26, p. 351–354, doi: 10.1130/0091-7613(1998)026<0351:RFIBLF>2.3.CO;2.

Lewis-Kenedi, C.B., Lange, R.A., Hall, C.M., and Delgado-Granados, H., 2005, The eruptive history of the Tequila volcanic field, western Mexico: Ages, volumes, and relative proportions of lava types: Bulletin of Volcanology, v. 67, p. 391–414, doi: 10.1007/s00445-004-0377-3.

Martinson, D.G., Pisias, N.G., Hays, J.D., Imbrie, J., Moore, T.C., Jr., and Shackleton, N.J., 1987, Age dating and the orbital theory of the Ice Ages—Development of a high-resolution 0 to 300,000-year chronostratigraphy: Quaternary Research, v. 27, p. 1–29, doi: 10.1016/0033-5894(87)90046-9.

Mathews, W.H., 1947, "Tuyas," flat-topped volcanoes in northern British Columbia: American Journal of Science, v. 245, p. 560–570.

McKnight, S.B., and Bacon, C.R., 1992, Olivine speedometry of multi-state magma mixing at Williams Crater, Crater Lake, Oregon: Geological Society of America Abstracts with Programs, v. 24, no. 5, p. 69.

Nakada, S., Bacon, C.R., and Gartner, A.E., 1994, Origin of phenocrysts and compositional diversity in pre-Mazama rhyodacite lavas, Crater Lake, Oregon: Journal of Petrology, v. 35, p. 127–162.

Nathenson, M., Bacon, C.R., and Ramsey, D.W., 2006, Subaqueous geology and a filling model for Crater Lake, Oregon: Hydrobiologia (in press).

Nelson, C.H., Bacon, C.R., Robinson, S.W., Adam, D.P., Bradbury, J.P., Barber, J.H., Jr., Schwartz, D., and Vagenas, G., 1994, The volcanic, sedimentologic and paleolimnologic history of the Crater Lake caldera floor, Oregon—Evidence for small caldera evolution: Geological Society of America Bulletin, v. 106, p. 684–704, doi: 10.1130/0016-7606(1994)106<0684:TVSAPH>2.3.CO;2.

Rieck, H.J., Sarna-Wojcicki, A.M., Meyer, C.E., and Adam, D.P., 1992, Magnetostratigraphy and tephrochronology of an upper Pliocene to Holocene record in lake sediments at Tulelake, northern California: Geological Society of America Bulletin, v. 104, p. 409–428, doi: 10.1130/0016-7606(1992)104<0409:MATOAU>2.3.CO;2.

Ritchey, J.L., 1980, Divergent magmas at Crater Lake, Oregon: Products of fractional crystallization and vertical zoning in a shallow, water-undersaturated chamber: Journal of Volcanology and Geothermal Research, v. 7, p. 373–386, doi: 10.1016/0377-0273(80)90039-6.

Rosenbaum, J.G., and Reynolds, R.L., 2004, Record of late Pleistocene glaciation and deglaciation in the southern Cascade Range, II. Flux of glacial flour in a sediment core from Upper Klamath Lake, Oregon: Journal of Paleolimnology, v. 31, p. 235–252, doi: 10.1023/B:JOPL.0000019229.75336.7a.

Sherrod, D.R., and Smith, J.G., 1990, Quaternary extrusion rates of the Cascade Range, northwestern United States and southern British Columbia: Journal of Geophysical Research, v. 95, p. 19,465–19,474.

Singer, B.S., Thompson, R.A., Dungan, M.A., Feeley, T.C., Nelson, S.T., Pickens, J.C., Brown, L.L., Wulff, A.W., Davidson, J.P., and Metzger, J., 1997, Volcanism and erosion during the past 930 k.y. at the Tatara–San Pedro complex, Chilean Andes: Geological Society of America Bulletin, v. 109, p. 127–142, doi: 10.1130/0016-7606(1997)109<0127:VAEDTP>2.3.CO;2.

Sisson, T.W., and Bacon, C.R., 1999, Gas-driven filter pressing in magmas: Geology, v. 27, p. 613–616, doi: 10.1130/0091-7613(1999)027<0613:GDFPIM>2.3.CO;2.

Sisson, T.W., and Grove, T.L., 1993, Experimental investigations of the role of H_2O in calc-alkaline differentiation and subduction zone magmatism: Contributions to Mineralogy and Petrology, v. 113, p. 143–166, doi: 10.1007/BF00283225.

Smellie, J.L., 2000, Subglacial eruptions, *in* Sigurdsson, H., Houghton, B.F., McNutt, S.R., Rymer, H., and Stix, J., eds., Encyclopedia of Volcanoes: San Diego, Academic Press, p. 403–418.

Stacey, J.S., Sherrill, N.D., Dalrymple, G.B., Lanphere, M.A., and Carpenter, N.V., 1981, A five-collector system for the simultaneous measurement of argon isotope ratios in a static mass spectrometer: International Journal of Mass Spectrometry and Ion Physics, v. 39, p. 167–180, doi: 10.1016/0020-7381(81)80031-9.

Stirling, C.H., Esat, T.M., Lambeck, K., and McCulloch, M.T., 1998, Timing and duration of the Last Interglacial—Evidence for a restricted interval of widespread coral reef growth: Earth and Planetary Science Letters, v. 160, p. 745–762, doi: 10.1016/S0012-821X(98)00125-3.

Stuiver, M., Reimer, P.J., and Braziunas, T.F., 1998, High-precision radiocarbon age calibration for terrestrial and marine samples: Radiocarbon, v. 40, p. 1127–1151.

Suzuki-Kamata, K., Kamata, H., and Bacon, C.R., 1993, Evolution of the caldera-forming eruption at Crater Lake, Oregon, indicated by component analysis of lithic fragments: Journal of Geophysical Research, v. 98, p. 14,059–14,074.

Thouret, J.-C., Finizola, A., Fornari, M., Legeley-Padovani, A., Suni, J., and Frechen, M., 2001, Geology of El Misti volcano near the city of Arequipa, Peru: Geological Society of America Bulletin, v. 113, p. 1593–1610, doi: 10.1130/0016-7606(2001)113<1593GOEMVN>2.0.CO;2.

Wentworth, C.M., and Fitzgibbon, T.T., 1991, ALACARTE user manual: U.S. Geological Survey Open-File Report 91-587C, version 1.0.

Williams, H., 1941, Calderas and their origin: Berkeley, California, University of California Publications, Bulletin of the Department of Geological Sciences, v. 25, no. 6, p. 239–346.

Williams, H., 1942, The geology of Crater Lake National Park, Oregon: Carnegie Institution of Washington Publication 540, 162 p.

Young, S.R., 1990, Physical volcanology of Holocene airfall deposits from Mt. Mazama, Crater Lake, Oregon [Ph.D. thesis]: Lancaster, UK, University of Lancaster, 307 p.

Zdanowicz, C.M., Zielinski, G.A., and Germani, M.S., 1999, Mount Mazama eruption: Calendrical age verified and atmospheric impact assessed: Geology, v. 27, p. 621–624, doi: 10.1130/0091-7613(1999)027<0621:MMECAV>2.3.CO;2.

Manuscript Received 30 September 2005
Revised Manuscript Received 4 April 2006
Manuscript Accepted 4 June 2006

Printed in the USA

Geological Society of America Bulletin

Eruptive history and geochronology of Mount Mazama and the Crater Lake region, Oregon

Charles R. Bacon and Marvin A. Lanphere

Geological Society of America Bulletin 2006;118, no. 11-12;1331-1359
doi: 10.1130/B25906.1